

STRUCTURAL AND DYNAMICAL PROPERTIES OF ORGANIC AND POLYMERIC
SYSTEMS USING MOLECULAR DYNAMICS SIMULATIONS

A Dissertation

Submitted to the Faculty

of

Purdue University

by

Leidy Lorena Alzate-Vargas

In Partial Fulfillment of the

Requirements for the Degree

of

Doctor of Philosophy

December 2019

Purdue University

West Lafayette, Indiana

**THE PURDUE UNIVERSITY GRADUATE SCHOOL
STATEMENT OF DISSERTATION APPROVAL**

Dr. Alejandro Strachan, Chair

School of Materials Engineering

Dr. James M. Caruthers

School of Chemical Engineering

Dr. R. Byron Pipes

School of Aeronautics and Astronautics

Dr. David Johnson

School of Materials Engineering

Approved by:

Dr. David F. Bahr

Head of the Departmental Graduate Program

*To my parents, Silvia and Eleazar for their love and unconditional support
and to my brother and most beloved friend, Juan Pablo*

ACKNOWLEDGMENTS

I would like to express my sincere gratitude to my advisor, Alejandro Strachan, in whom I have found a role model and constant support in my personal and professional development. I am thankful for his patience and persistence for me to be a successful scientist. I would like to thank my committee members James Caruthers, Byron Pipes and David Johnson for their observations and suggestions during my preliminary examinations.

A special appreciation to my undergraduate professors Jorge David and Mario Vélez, who pushed me to pursue a career in science and ultimately to embark in the Ph.D. and to Nicolas Onofrio for his valuable mentorship and guidance that helped me in learning how to be a better researcher.

I would like to thank all the past and current Strachan's group members, specially Chunyu Li, David Guzman, Samuel Reeve, Tongtong Shen and Saaketh Desai for their suggestions and collaborations.

Special thanks to the wonderful friends I made during this journey, Gustavo Valencia, Nelyan López, Ángel Monroy and Daniel Valencia. Their support and companionship is very valuable to me.

I am deeply thankful to my family: my parents, brother, grandparents and all my relatives for their love and support during my years at Purdue and for always cheering me when I most needed. Last but not least, my most sincere gratitude to Gregorio Hernández for his endless caring and love.

TABLE OF CONTENTS

| | Page |
|--|------|
| LIST OF TABLES | vii |
| LIST OF FIGURES | viii |
| ABBREVIATIONS | xii |
| ABSTRACT | xiii |
| CHAPTER 1. INTRODUCTION | 1 |
| 1.1 The Glass Transition Temperature | 5 |
| CHAPTER 2. THEORETICAL BACKGROUND | 10 |
| 2.1 Classical Molecular Dynamics | 10 |
| 2.1.1 Statistical Mechanics Basic Concepts | 10 |
| 2.1.2 Equations of Motion | 11 |
| 2.1.3 Force Fields | 13 |
| 2.2 Setting Up a Molecular Dynamics Simulation | 17 |
| 2.2.1 Structure to LAMMPS | 17 |
| 2.2.2 Building a Structure | 19 |
| CHAPTER 3. UNCERTAINTIES IN PREDICTED THERMO-PHYSICAL PROP- ERTIES OF THERMOPLASTIC POLYMERS USING MOLECULAR DYNAMICS | 20 |
| 3.1 Introduction | 20 |
| 3.2 Simulation Details | 22 |
| 3.2.1 Molecular Systems | 22 |
| 3.2.2 Amorphous Structure Generation | 23 |
| 3.2.3 Molecular Dynamics Simulations | 24 |
| 3.2.4 Data Analysis procedure | 25 |
| 3.2.5 Conformational transition analysis | 27 |
| 3.3 Predictions and Comparison Against Experiments | 28 |
| 3.3.1 Role of Builder, Molecular Weight, Force Field and Data Analysis on Predicted Quantities | 33 |
| 3.4 Physical Origin of the Trends in Predictions | 37 |
| 3.4.1 Amorphous builder | 38 |
| 3.4.2 Force Field | 39 |
| 3.5 Glass Transition Notebook | 43 |
| 3.6 Conclusions | 45 |
| CHAPTER 4. MOLECULAR MODELING OF SMALL ORGANIC CRYSTALS | 46 |
| 4.1 Introduction | 46 |
| 4.2 Simulation Details | 47 |

| | Page |
|--|------|
| 4.3 Predicted Properties in Organic Crystals | 48 |
| 4.4 Conclusions | 53 |
| CHAPTER 5. LOCAL CHAIN DYNAMICS AND GLASS TRANSITION IN POLY- MERIC BULK AND FINITE SIZE SYSTEMS BY MOLECULAR DYNAMICS SIMULATIONS | 54 |
| 5.1 Introduction | 54 |
| 5.2 Computational Details | 55 |
| 5.2.1 Polymeric Systems | 55 |
| 5.2.2 Molecular Dynamics Simulations | 56 |
| 5.2.3 Torsional Transition Analysis | 57 |
| 5.2.4 Cluster Analysis | 58 |
| 5.3 Torsional Relaxation in Bulk Systems | 59 |
| 5.4 Role of Chain Molecular Weight and Size Effects in Torsional Relaxation . . . | 70 |
| 5.5 Universality of Critical Exponents from High-Mobility Domains | 74 |
| 5.6 Conclusions | 75 |
| REFERENCES | 76 |
| VITA | 84 |

LIST OF TABLES

| Table | Page |
|--|------|
| 2.1 Important statistical ensembles used in molecular dynamics simulations. Adapted from "From Atoms to Materials: Predictive Theory and Simulations" [39] | 12 |
| 3.1 Predicted densities at room temperature, glass transition temperatures and coefficient of thermal expansion for poly(methyl-metacrylate) systems | 31 |
| 3.2 Predicted densities at room temperature, glass transition temperatures and coefficient of thermal expansion for polystyrene systems | 32 |
| 4.1 Predicted MD lattice parameters and experimental values for various small organic crystals | 49 |
| 5.1 Predicted glass transition temperatures T_g [K] from MD simulations for bulk samples using two fitting procedures | 60 |

LIST OF FIGURES

| Figure | Page |
|---|------|
| 1.1 Design of new organic light-emitting diodes using combined theoretical and computational approaches, and experimental characterization. Adapted with permission from Ref. [4] © 2016 Springer Nature | 2 |
| 1.2 Volume vs. Temperature for a hypothetical system in the liquid, crystalline and, glassy state. If the system becomes a glass, the glass transition temperature T_g is determined by the change in the slope from the V vs. T data. | 3 |
| 1.3 $G(t)$ modulus or relaxation function at the glass transition region showing the main relaxation process involved: segmental or cooperative α from the motion of several segments e.g. the rotation of torsions along backbone chain, and secondary process β involving small vibrational motions | 6 |
| 1.4 Sketch of dynamic heterogeneities showing the time scale of fluctuations of rates and length scale ξ_{het} of slow clusters. Reproduced with permission from Ref. [26] © 1998 The American Physical Society | 7 |
| 2.1 Structure of a minimalist molecular dynamics code. Reproduced from “From Atoms to Materials: Predictive Theory and Simulations” [53] | 14 |
| 2.2 Schematic of a simple chain molecule including bond r , bend angle θ and torsion angle ϕ . Reproduced from “Introduction to Molecular Dynamics Simulation” . . . | 15 |
| 2.3 Schematic of the methodology implemented in the LAMMPS Data File Generator tool | 18 |
| 2.4 Snapshot of the LAMMPS Data File Generator tool, available in nanoHUB. The tool can be used to convert atomic and molecular structures into a LAMMPS data file containing all the connectivity and force field terms required to run a MD simulation | 18 |
| 3.1 Schematic of the methodology implemented in the present work | 22 |
| 3.2 Estimates of T_g (red point) from a single simulation using two fitting procedures: (a) T_g is estimated as the intersection of low (blue) and high (green) temperature best-fit lines and (b) Hyperbola (red) fit to the data, here T_g is estimated from the intersection of the asymptotes (dashed blue) | 26 |

| Figure | Page |
|---|------|
| 3.3 Glass transition T_g (MD Ave) and density at 300 K for different input choices. Filled symbols represent predicted values using bilinear fitting method, empty symbols represent values obtained with the hyperbola method. Predictions are circled in orange for PMMA and blue for PS, light colored ellipses refer to experimental data whereas dark colored ellipses represent WLF-corrected experimental data. | 28 |
| 3.4 Predicted glass transition temperatures for each combination of input choices in polymer samples (a) PMMA and (b) PS. All PS simulations are performed by generating samples with the same amorphous builder method | 29 |
| 3.5 Differences in predicted values for each of the quantities of interest originating from each of the independent variables studied. Red bars represent QoI Ave and hashed bars represent MD Ave | 34 |
| 3.6 Density vs temperature plot for combination: PMMA, 700 monomers, SARW, PCFF. This case results in a large variation for predicted T_g depending on the data analysis used. Predicted glass transition using bilinear fit shown in red and in blue for hyperbola fit method | 36 |
| 3.7 Estimates of T_g for PMMA bulk samples with bilinear method (solid bars) and hyperbola method (hashed bars) according to the upper temperature regime used in the regression | 37 |
| 3.8 Comparison of predicted properties within the two builders in PMMA systems with 70 monomers. (a) Density vs temperature, inset: difference in density between SARW and CBMC as a function of temperature (b) Conformational transition rate normalized per torsion and time vs temperature, inset: transition rate difference between SARW and CBMC as a function of temperature (c) Radii of gyration vs temperature | 38 |
| 3.9 Distribution of backbone torsional angles from MD simulations for PMMA and PS, above T_g : 550 K and below T_g : 200 K | 40 |
| 3.10 Conformational transition rates for each force field as a function of temperature for structures built with CBMC; <i>left</i> PMMA; <i>right</i> PS | 41 |
| 3.11 R_g distribution averaged over the five samples built with the CBMC method and 10 chains for both polymers from MD simulations; <i>left</i> PMMA and <i>right</i> PS | 42 |
| 3.12 Radial distribution functions at 300 K as a function of the force field for a sample with 10 chains; <i>left</i> PMMA and <i>right</i> PS | 42 |
| 3.13 Snapshots of the Glass Transition Notebook as displayed at nanoHUB including the visualization of built polymer system and results | 44 |
| 4.1 Crystalline structure of compounds F1 and F2 | 47 |
| 4.2 γ -indomethacin crystal and amorphous structures and density changes during heating and cooling with predicted glass transition and melting temperature . . . | 50 |

| Figure | Page |
|--|------|
| 4.3 Coexistence of crystal and amorphous structures and the determination of melting temperature in γ -indomethacin | 51 |
| 4.4 Calculated amorphization enthalpy from MD simulations | 52 |
| 4.5 Validation of predicted properties using MD for various small organic crystals (a) density at room temperature, (b) melting temperature, and (c) enthalpy of fusion | 52 |
| 5.1 Torsional transition analysis. (a) Time evolution of a backbone dihedral angle obtained from the MD trajectory every 0.1 ps (red line). A window average has been performed to obtain a torsional angle every 2 ps shown as black line. (b) Jumps detected for the monitored angle. (c) All transitions (black points) found for backbone dihedral angles as a function of time in bulk PMMA at 480K . . . | 57 |
| 5.2 Cluster analysis procedure visualization. Two clusters of active torsions (C1 and C2) are detected within space cutoff at $t = 2$ ps, at consecutive times (until reaching cutoff) we monitored the same torsions and nearby ones so they will be included in initial identified clusters | 58 |
| 5.3 Active backbone torsions as a function of time in PMMA at 480K after clustering analysis. Each color represents a cluster identified in the simulation, however torsion index does not represent the location in space of the dihedral angles . . . | 59 |
| 5.4 Density vs. temperature data for each polymer and computed glass transition temperature. Solid lines and dashed lines represent results from the bilinear and hyperbola fitting procedure respectively | 60 |
| 5.5 Conformational transition rates as a function of temperature for bulk polymeric samples. (a) Torsional transition rates vs. temperature; shadow regions represent glass transition regimes and, (b) Transition rates as a function of temperature in Arrhenius form for each polymer | 61 |
| 5.6 Activation energy (E_a) from backbone torsions as a function of bulk T_g | 62 |
| 5.7 Snapshots of bulk polystyrene at 460 K with active torsions in yellow. The blue points represent the torsion centers along the backbone chain | 63 |
| 5.8 Radial distribution function of backbone torsions in bulk PMMA at 450 K, PS at 450 K, PP at 260 K, and PE at 200 K | 64 |
| 5.9 Torsional transition rates $\ln k$ with respect to cluster size vs. temperature $1000/T$ for bulk polymers using $t_c = 64$ ps. The predicted T_g s from bilinear and hyperbola fits and the averaged value are shown as dashed lines | 65 |
| 5.10 Average cluster size defined as number of torsions normalized per time over all clusters in log-scale (black points) corresponding to $t_c = 64$ ps and defined R_c for bulk samples. Colored points show the distribution of cluster sizes per time as a function of temperature. Size of a mobile cluster grows as $T \rightarrow T_g$ in concordance with the percolation behavior | 66 |

| Figure | Page |
|---|------|
| 5.11 Average cluster lifetime (last time active torsion - first time active torsion) in black points. The distribution of cluster duration is shown in colors | 66 |
| 5.12 Largest cluster normalized by active torsions as a function of temperature at different t_c using selected distance cutoff | 67 |
| 5.13 Strength of largest cluster normalized by active torsions as a function of temperature for bulk polymeric samples. clustering analysis performed with various time and spatial cutoffs. The critical temperature for percolation of clusters is around the glass transition temperature across all samples | 68 |
| 5.14 Torsions in order of appearance as a function of time, colored by cluster in temperatures near T_g in bulk samples; (a) PMMA, (b) PS, (c) PP and, (d) PE | 69 |
| 5.15 (a) Density vs. Temperature for bulk samples of 40 chains and 4 chains and slab system with 40 chains of PMMA, and (b) Arrhenius plot of conformational transition rates vs temperature for PMMA samples | 70 |
| 5.16 Largest cluster normalized by active torsions as a function of temperature at different time cutoffs with spatial correlation for poly(methyl-methacrylate) samples including finite size geometries | 71 |
| 5.17 Cluster evolution in the vicinity of T_g for PMMA samples. Torsion index labeled in order of appearance in time | 73 |
| 5.18 Critical exponents in percolation of high-mobility domains for (a) bulk polymers and (b) PMMA samples | 74 |

ABBREVIATIONS

| | |
|--------|---|
| MD | Molecular Dynamics |
| LAMMPS | Large-scale Atomic/Molecular Massively Parallel Simulator |
| PCFF | Polymer Consistent Force Field |
| CBCM | Configurational Bias Monte Carlo |
| SARW | Self-Avoiding Random Walk |
| RDF | Radial Distribution Function |
| NMR | Nuclear Magnetic Resonance |
| BDS | Broadband Dielectric Spectroscopy |
| AFM | Atomic Force Microscopy |
| CRR | Cooperatively Rearranging Region |
| DH | Dynamic Heterogeneity |
| QoI | Quantity of Interest |

ABSTRACT

Alzate-Vargas, Lorena Ph.D., Purdue University, December 2019. Structural and Dynamical Properties of Organic and Polymeric Systems using Molecular Dynamics Simulations. Major Professor: Alejandro Strachan.

The use of atomistic level simulations like molecular dynamics are becoming a key part in the process of materials discovery, optimization and development since they can provide complete description of a material and contribute to understand the response of materials under certain conditions or to elucidate the mechanisms involved in the materials behavior. We will discuss to cases in which molecular dynamics simulations are used to characterize and understand the behavior of materials: i) prediction of properties of small organic crystals in order to be implemented in a multiscale modeling framework which objective is to predict mechanically induced amorphization without experimental input other than the molecular structure and ii) characterization of temperature dependent spatio-temporal domains of high mobility torsions in several bulk polymers, thin slab and isolated chains; strikingly we observe universality in the percolation of these domains across the glass transition.

However, as in any model, validation of the predicted results against appropriate experiments is a critical stage, especially if the predicted results are to be used in decision making. Various sources of uncertainties alter both modeling and experimental results and therefore the validation process. We will present molecular dynamics simulations to assess uncertainties associated with the prediction of several important properties of thermoplastic polymers; in which we independently quantify how the predictions are affected by several sources. Interestingly, we find that all sources of uncertainties studied influence predictions, but their relative importance depends on the specific quantity of interest.

1. INTRODUCTION

The continuous need of advanced high-performance materials has challenged the scientific and engineering communities in order to accelerate their discovery, design, and deployment. The Materials Genome Initiative MGI launched in 2011 [1,2] provided a framework to encompass the integration of computational tools, experimental tools and digital data, such as materials databases or informatics, to achieve a fast and reliable discovery and deployment of low-cost materials.

Successful examples of advances in materials science using the MGI include the combination of experimental data and physics-based models to develop polymeric self-assembly systems, [3] and the discovery of cost-effective molecules organic light-emitting diodes (OLED) by combining theory, computational quantum chemistry and experiments, [4] see Figure 1.1 for the implemented workflow used in the later case. Therefore, simulation tools that enable predicting materials properties and behavior from first principles are becoming a key part in the process of materials development continuum.

From the wide range of materials that have been studied using simulation techniques, polymeric and organic materials are of particular interest due to their wide variety of applications; from large-scale high-temperature composite matrices and heat shields used in the aerospace industry to conducting polymers at nano-scale devices, flexible displays and packaging. Glassy polymers are key for a broad variety of industry and technological uses. Many include fuselage in airplanes, [5] nano-devices where polymer is used as a substrate or sometimes as a dielectric, [6] and nano-composites for the automotive and aviation industries. [7] Consequently, understanding and predicting the long-term behaviour of polymers in the glassy state remains of great interest.

The implementation of atomistic simulations like molecular dynamics can provide a com-

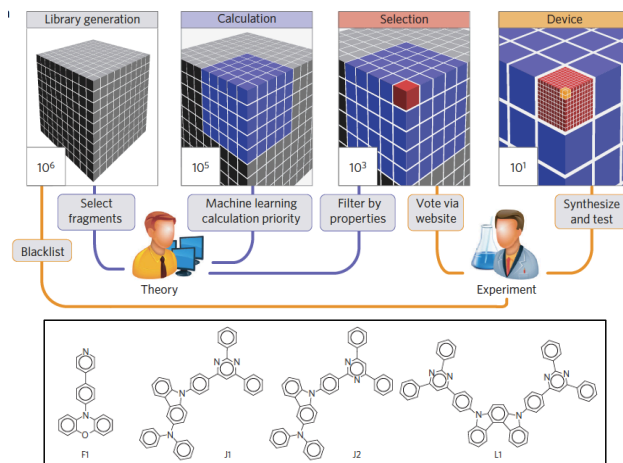


Figure 1.1.: Design of new organic light-emitting diodes using combined theoretical and computational approaches, and experimental characterization. Adapted with permission from Ref. [4] © 2016 Springer Nature

plete description of organic systems and contribute to understanding the response of materials under specific conditions, and the mechanisms involved in their behavior. As a result, MD simulations have been often used to predict properties and explore organic materials whose properties such as structural, thermal or, mechanical show potential and can help designing new complex materials, deserving further experimental studies.

However, the limitations of a model can result in discrepancies during the validation process between experiments and simulation, originating from a variety of uncertainty sources that must be considered in order to assess confidence in the predictions delivering sufficient information for decision making. In crystalline materials where predicted properties can be computed at the unit cell level using DFT, the uncertainties and reproducibility in such calculations are well understood. [8] Properties susceptible to such treatment include those that depend weakly on microstructure such as elastic or dielectric constants, defect energies or band gaps where DFT or beyond-DFT methods offer the required accuracy for a range of materials. Some examples of proposed new materials using DFT where validation has been considered, include materials for photoelectrochemical devices [9] and doping

avenues for single layer transition metal dichalcogenides [10].

Unlike the previously described cases, the prediction of properties that depend on materials processing and molecular structure using computational atomistic tools is more complex, since the coupling of various models is often needed to describe structure and hence, the properties of interest. In polymers, for example, molecular properties can be influenced by molecular weight, backbone and side-chains stiffness. It is often the case that uncertainties in these models are poorly understood and can vary significantly from material to material and from property to property, arising the question of whether a simulation result is reliable enough.

If we think in a molecular simulation of a polymer, we must consider: (i) molecular weight of the samples, (ii) amorphous generation method, (iii) force field used to describe atomic interactions, (iv) the analysis used to extract the quantities of interest.

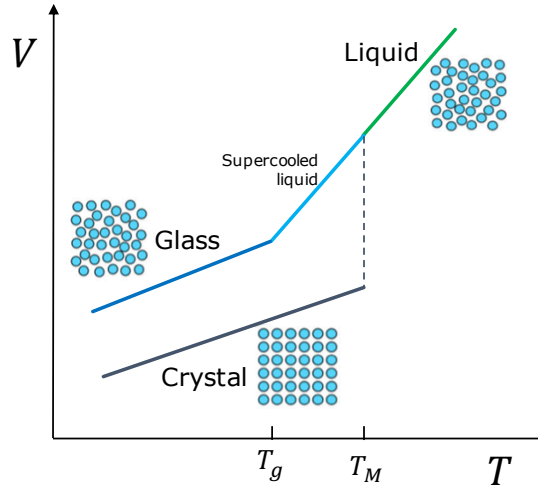


Figure 1.2.: Volume vs. Temperature for a hypothetical system in the liquid, crystalline and, glassy state. If the system becomes a glass, the glass transition temperature T_g is determined by the change in the slope from the V vs. T data.

One of the critical properties in glassy polymers is the glass transition temperature T_g . In polymer physics, this is the temperature in which a liquid transitions into a glassy

form and becomes soft. A glass is an amorphous solid, i.e. it lacks the periodicity and long-range order; more importantly, the glass is in a state of non-equilibrium, differing from liquids and crystals as it is shown in Figure 1.2; further discussion in this matter will be addressed in 1.1. Several works understanding the effect of molecular weight, cooling rate and data analysis in T_g have been done independently. [11, 12] In the last-mentioned case, following the general consensus in terms of accessing the glass transition temperature from examination of volume V (or density ρ) vs. temperature T , and defined as the change in the slope between the low and high temperature regimes, see Fig. 1.2; Patrone et al. (2016) proposed an uncertainty quantification (UQ) methodology of data analysis for glass transition temperature in polymers, [12] that consisted in a hyperbola-based regression [13] to fit the ρ vs. T data to find T_g . The main goal was to yield a consensus value by weighting the estimates from all possible outcomes of multiple density vs. temperature datasets obtained in a simulation. With their set of analysis, it was possible to combine small simulations to agree on estimates with uncertainties comparable to larger simulations, nevertheless quantification of other uncertainties built into the MD algorithm or arising from simulation in polymers is omitted.

Because of the lack of works that address the uncertainties in simulated predictions of some properties and the effect of several factors in the simulation, we propose a systematic methodology involving state-of-the-art molecular simulations of well known glassy polymeric systems to predict key quantities relevant to these materials, including the glass transition temperature. It will be later demonstrated that all sources of uncertainties studied (molecular weight, amorphous builder, force field and data analysis) influence the predictions, depending significantly on the quantity of interest. We expect that this comprehensive work will contribute in establishing adequate practices for molecular modeling of polymeric materials that can lead to confident predictions and elucidation of characteristic materials behavior.

1.1 The Glass Transition Temperature

Understanding the glass phenomenon and the implications in polymer's behavior is a subject of high interest in science. From an applied point of view, understanding the glass transition is critical to determine operational ranges and fabrication sizing in order to avoid property degradation.

Several physical phenomena and materials properties evolve significantly during the phase transformation happening at the glass transition. [14] As the temperature is reduced through the glass transition temperature, there is a drastic increase in the viscosity η of the material (reaching about 10^{13} poise), [15] eventually turning into a, often brittle, solid. Consequent with the increase in viscosity, in polymers, chain relaxation dynamics and time through the glass transition, referred to as the α -relaxation process, slows down dramatically by more than 10 orders of magnitude.

Despite significant work several questions remain debatable; what kinds of changes occur in the molecular structure of polymers when crossing T_g ? what is the relationship between molecular mobility and the slowing of the α -relaxation dynamics at the glass transition region?

Relaxation Process in Polymers We already introduced the concept of α -relaxation, however it is important to clarify that two main relaxation processes are identified at the glass transition region: α and β . These relaxations are involved with chain motion in polymers as shown in Figure 5.3. The α process (also called cooperative process) is caused by the rearrangement of many repeating units and mainly associated to the glass transition phenomena; a secondary, very fast relaxation process β , connected to the vibration and reorientation of small groups of atoms (i.e. the side group rotates about the bond linking it to the main chain), becomes relevant just below T_g .

Adams and Gibbs (1965) [16] introduced in early 1960's the concept of *Cooperatively Rearranging Region* CRR as the the smallest subsystem that can rearrange into another

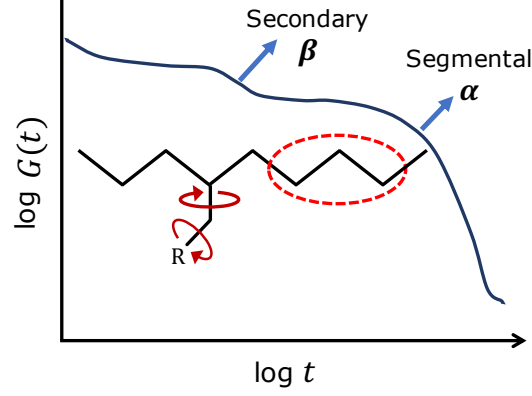


Figure 1.3.: $G(t)$ modulus or relaxation function at the glass transition region showing the main relaxation process involved: segmental or cooperative α from the motion of several segments e.g. the rotation of torsions along backbone chain, and secondary process β involving small vibrational motions

configuration, a key process for the relaxation at T_g . It introduced as well, the idea of dynamic heterogeneities (DHs), understood as domains that exhibit faster dynamics than other regions only few nanometers away in a glassy material. A visual representation of the DH concept is displayed in Fig. 1.4. Experimental [17, 18] and computational [19–25] studies have reveal the existence of heterogeneous behavior in supercooled liquids as the glass transition temperature is approached, thus, several questions have emerged; how large are these domains and how long do they last? And even more intriguing, what is the origin of those heterogeneities?

In an attempt to answer those questions, modern experimental techniques have been used, achieving the characterization of DHs in several materials. Spiess & coworkers performed solid-state nuclear magnetic resonant (NMR) measurements on poly(vinyl acetate) to confirm the existence of heterogeneities and determined the characteristic size about 3 ± 1 nm at $T_g + 10$ K. [26] With the same technique, it was found the size of dynamic heterogeneities to be about 2.5 nm in poly(methyl methacrylate) and 3.3 nm in polystyrene. [27]

Other experimental techniques such as atomic force microscopy (AFM) [24, 28] and photo-bleaching, [17] estimated the lifetime of dynamic heterogeneous domains in several

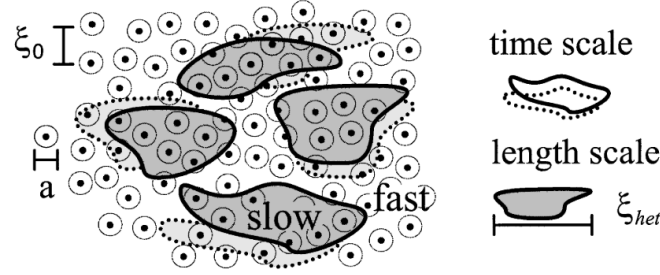


Figure 1.4.: Sketch of dynamic heterogeneities showing the time scale of fluctuations of rates and length scale ξ_{het} of slow clusters. Reproduced with permission from Ref. [26] © 1998 The American Physical Society

glass-formers to be on the order of 10^1 to 10^4 s around T_g . Broadband dielectric spectroscopy (BDS) [29–31] and fluorescence spectroscopy studies [32] have been carried out to explore the α -relaxation dynamics and their characteristic times in polymers. Other indirect methods such as the multi-point dynamic susceptibility function [33, 34] have been used extensively to study the dynamic heterogeneities. There is general consensus that the characteristic size of the cooperative regions is in the range 1-5 nm for a wide range of glass-formers at the glass transition. [33, 35–37]

Glass Transition and Relaxation Dynamics in Films and Single Molecules

In the interest of the large number of technological applications existent that require free surfaces or interfaces, for example: opto/electromechanical devices at micro and nano-scale, or biomedical sensors; it is common to ask, how much does the dynamics of a polymer under confinement or the presence of free surfaces near the glass transition differs from the bulk?. However, in spite of the great advances in experimental methods, the relaxation dynamics in non-bulk polymers remain contradictory.

Priestley et al. (2005) [32] used a fluorescence technique to determine the glassy-state relaxation dynamics of poly(methyl methacrylate) (PMMA) films in a set of multilayer

configurations with the objective to study the effect of confinement. Interestingly, it was found an enhancement of mobility near polymer free surface that leads in reduction of T_g . Other works in polystyrene (PS) have confirmed the existence of a mobile layer [38–40] with a bulk-like interior region. [41] Using the same polymer, the time evolution of DHs in films has been studied by means of atomic force microscopy. Consistent with the existence of a thin liquid-layer at the glassy surface observed in many experiments, it was determined that the length scale of the heterogeneities was ~ 2.1 nm, with a lifetime of $\sim 10^2$ s; [24] in agreement with reported values for bulk polymers around the glass transition. On the other hand, Tress et al. (2010) [30] using BDS experiments found that dynamics of layers down to 5 nm do not deviate from bulk-like glassy dynamics and glass transition does not exceed margins of ± 3 K.

Surprisingly, studies of glassy dynamics in isolated and semi-isolated chains using broadband dielectric spectroscopy [31] revealed a lack of size dependence in the α –relaxation. The dynamics of the studied chains have insignificant deviations (statistically) from the bulk behavior, since the length scale of the cooperative process required for the glass transitions is about 2-3 polymer segments, a much smaller size relative to the chain size ~ 50 nm.

Numerous large molecular dynamics simulations of supercooled Lennard-Jones liquids [21–23, 42–44] have reaffirmed the existence of spatially heterogeneous dynamics by characterizing mobile particles. It was possible to identify regions in the sample where the local structure has remained constant through the simulation, concurrently, other regions rearranged significantly. Baljon et al. (2004) [45] studied the glass transition of supported polymer films, and they confirmed percolation of immobile domains around the glass transition temperature. Yet, two limitations need to be stated; first, these simulations have simplified molecular structure and smaller molecular weights than in experiments, and second, relaxation times are limited, some roughly achieve 100 ns, whereas typical experimental times are on the order of seconds.

In amorphous polymers, MD simulations have focused on describing the motion of torsional angles i.e. conformational transitions to characterize the dynamics at the glass transition. [46–51] Since they can provide atomistic detailed information corresponding to structural changes along the polymer. Wu et al. studied the conformational changes of polyethylene bulk samples [52] and poly(vinylidene fluoride), [52] discerning two different Arrhenius behaviors in the transition rates, their intersection successfully predicted T_g . They also observed heterogeneous behavior in the torsional rates as temperature approaches the glass transition as a result of atoms being “frozen”. However, the nature of the spatio-temporal domains from conformational transitions in polymer systems has not been addressed.

In order to understand the cooperative motion of torsions in the bulk polymers and systems with free surfaces, molecular dynamics simulations will be used to characterize high-mobility domains of torsions along backbone chain and the universal percolation behavior of these domains across all samples.

To this end, this dissertation is organized as follows: a brief description of molecular dynamics is presented in Chapter 2. In Chapter 3 presents a study of the uncertainties associated to the prediction of several properties in thermoplastic polymers using MD simulations. In Chapter 4 the use of MD simulations in a multiscale framework to predict properties in small organic crystals is presented. Chapter 5 discusses MD simulations to identify and characterize spatio-temporal correlations in high-mobility torsions in polymers at the glass transition.

2. THEORETICAL BACKGROUND

*“Although this may seem a paradox,
all exact science is based on the idea of approximation.”*

- Bertrand Russell

2.1 Classical Molecular Dynamics

Molecular dynamics (MD) simulation is a powerful computational method that integrate the Newtonian equations of motion of a many-body system. *Classical* MD simulations have been widely used to describe and investigate the structure and thermodynamics of atomic systems from liquids, molecules and polymers to crystals. Given that statistical mechanics concepts are at the core of molecular dynamics theory, the next section (2.1.1) briefly introduces basic principles and in section 2.1.2 the equations of motion are discussed. In section 2.1.3 we will introduce the concept of empirical potential that constitutes the heart of a *classical* MD simulation.

2.1.1 Statistical Mechanics Basic Concepts

In molecular dynamics simulation, we often want to explore macroscopic properties based on microscopic simulations, for example, to calculate the energetics involved in conformational change. To connect a microscopic simulation with macroscopic properties, statistical mechanics expressions are implemented to solve equations of motion and to relate properties to the distribution and motion of the atoms of the many-body system.

Section 2.1 based on the online course “*From Atoms to Materials*” [53] by Alejandro Strachan from Purdue University, “*Introduction to Molecular Dynamics: Theory and Applications in Biomolecular Modeling*” [54] by Yi Wang and J. Andrew McCammon and “*Molecular Dynamics of Glassy Polymers*” [55] by Julian Clarke

Statistical Ensembles The collection of all possible systems that have different microscopic states (microstates) which all satisfy the conditions of a unique thermodynamic state such as temperature T , pressure P , volume V , energy E , and number of particles or atoms N . In MD simulation a sequence of points in space and time that belong to the same ensemble. An observable A can be calculated by averaging the value of such observable over the ensemble, i.e. $A_{\text{obs}} = \langle A \rangle_{\text{ens}}$, where $\langle A \rangle_{\text{ens}}$ is called an ensemble average of A . Some ensembles are listed below.

Microcanonical Ensemble The microcanonical ensemble (NVE) is characterized by a constant number of atoms, N , a fixed volume, V , and fixed energy, E . It is assumed that all systems of the ensemble are isolated and evolve independently.

Canonical Ensemble In the canonical ensemble (NVT) a collection of systems are in a thermodynamic state with a fixed number of atoms, N , a fixed volume, V , and constant temperature, T . The system of interest is embedded in a large system that behaves as a heat bath. Both systems interact by exchanging energy in the form of heat.

Isobaric/Isothermal Ensemble The isobaric-isothermal ensemble (NPT) maintains fixed number of atoms, N , constant pressure, P , and constant temperature, T . The system is described by the partition function of canonical ensemble in 3 dimensions.

In an MD simulation, we will be able to calculate an observable A as a time average from a simulation trajectory, $A_{\text{obs}} = \langle A \rangle_{\text{time}}$. Table 2.1 shows the probability distribution, partition function and free energy expressions for the statistical ensembles used in molecular dynamics previously mentioned.

2.1.2 Equations of Motion

The molecular dynamics simulation method is based on the equation of motion, $F = ma$. To start a simulation, initial positions and velocities of all atoms in the system are assigned; the forces on each atom are computed. Next, the temporal evolution of a

Table 2.1.

Important statistical ensembles used in molecular dynamics simulations. Adapted from "From Atoms to Materials: Predictive Theory and Simulations" [39]

| | Microcanonical (NVE) | Canonical (NVT) | Isobaric/Isothermal (NPT) |
|--------------------------|--|--|--|
| Probability Distribution | $P(\mathbf{r}, \mathbf{p}) = \frac{1}{\Omega(N, V, E)}$ | $P(\mathbf{r}, \mathbf{p}) = \frac{e^{-\beta H(\mathbf{r}, \mathbf{p})}}{Z_{NVT}}$ | $P(\mathbf{r}, \mathbf{p}, V) = \frac{e^{-\beta H(\mathbf{r}, \mathbf{p}) - PV}}{Z_{NPT}}$ |
| Partition Function | $\Omega(N, V, E) = \sum_{\text{states}} \delta(E - H(\mathbf{r}, \mathbf{p}))$ | $Z_{NVT} = \sum_{\text{states}} e^{-\beta H(\mathbf{r}, \mathbf{p})}$ | $Z_{NPT} = \sum_V \sum_{\text{states}} e^{-\beta H(\mathbf{r}, \mathbf{p}) - PV}$ |
| Free Energy | $S = k_B \log \Omega(N, V, E)$ | $F_{NVT} = -k_B T \log Z_{NVT}$ | $G_{NPT} = -k_B T \log Z_{NPT}$ |

simulation involves integrating the equations of motion for the particles according to their interaction, determined by $V(\mathbf{r})$; we will describe the implementation of this potential for polymeric materials in 2.1.3. The equations of motion are expressed as:

$$\begin{aligned}\dot{\mathbf{r}} &= \frac{\mathbf{p}}{m} \\ \dot{\mathbf{p}} &= \mathbf{F}\end{aligned}\tag{2.1}$$

where the force on each atom is:

$$\mathbf{F} = \nabla V(\mathbf{r})\tag{2.2}$$

As mentioned, $V(\mathbf{r})$ describes the interaction between atoms.

$$\begin{aligned}\dot{\mathbf{r}} &= \frac{\mathbf{p}}{m} = \frac{\mathbf{r}(t + \Delta t) - \mathbf{r}(t)}{\Delta t} \\ \dot{\mathbf{p}} &= \mathbf{F} = \frac{\mathbf{p}(t + \Delta t) - \mathbf{p}(t)}{\Delta t}\end{aligned}\tag{2.3}$$

if we rearrange:

$$\begin{aligned}\mathbf{r}(t + \Delta t) &= \mathbf{r}(t) + \frac{\mathbf{p}}{m} \cdot \Delta t \\ \mathbf{p}(t + \Delta t) &= \mathbf{p} + \mathbf{F} \cdot \Delta t\end{aligned}\tag{2.4}$$

Integration of these equations is done using the Verlet algorithm, which does a Taylor expansion of the position with respect to time. We could rewrite in different time directions:

$$\begin{aligned}\mathbf{r}(t + \Delta t) &= \mathbf{r}(t) + \dot{\mathbf{r}}(t)\Delta t + \frac{1}{2}\ddot{\mathbf{r}}(t)\Delta t^2 + \frac{1}{6}\ddot{\mathbf{r}}(t)\Delta t^3 + \mathcal{O}(\Delta t^4) \\ \mathbf{r}(t - \Delta t) &= \mathbf{r}(t) - \dot{\mathbf{r}}(t)\Delta t + \frac{1}{2}\ddot{\mathbf{r}}(t)\Delta t^2 - \frac{1}{6}\ddot{\mathbf{r}}(t)\Delta t^3 + \mathcal{O}(\Delta t^4)\end{aligned}\tag{2.5}$$

Figure 2.1 shows a schematic describing the fundamental loop that allows time evolution in a molecular dynamics simulation.

MD is deterministic which means that once the positions and velocities of each atom are known, the state of the system can be predicted at any time in the future or in the past. Molecular dynamics have been implemented in various simulation packages, with a variety of analysis methods integrated. In this work we use the Large-scale Atomic/Molecular Massively Parallel Simulator (LAMMPS) as our MD engine.

2.1.3 Force Fields

As we mentioned previously, we need to calculate the forces F_i acting on each atom; and these are usually obtained from the interatomic potential $V(\mathbf{r})$, often referred as *force field*. Force field parameters are usually estimated from experimental data or quantum mechanics calculations and optimized to reproduce materials properties. As forces have to be as realistic but also achievable, force fields constitute the heart of an MD algorithm.

There are many force fields available for MD simulations of polymeric and organic materials; two force fields will be used across this work: in the majority of the cases, simulations are performed using DREIDING force field. [56] We also introduced simulations using the Polymer Consistent Force Field (PCFF). [57]

Generally, interatomic potentials used for molecular modeling, and especially in soft materials, are composed of bonded and non-bonded interactions.

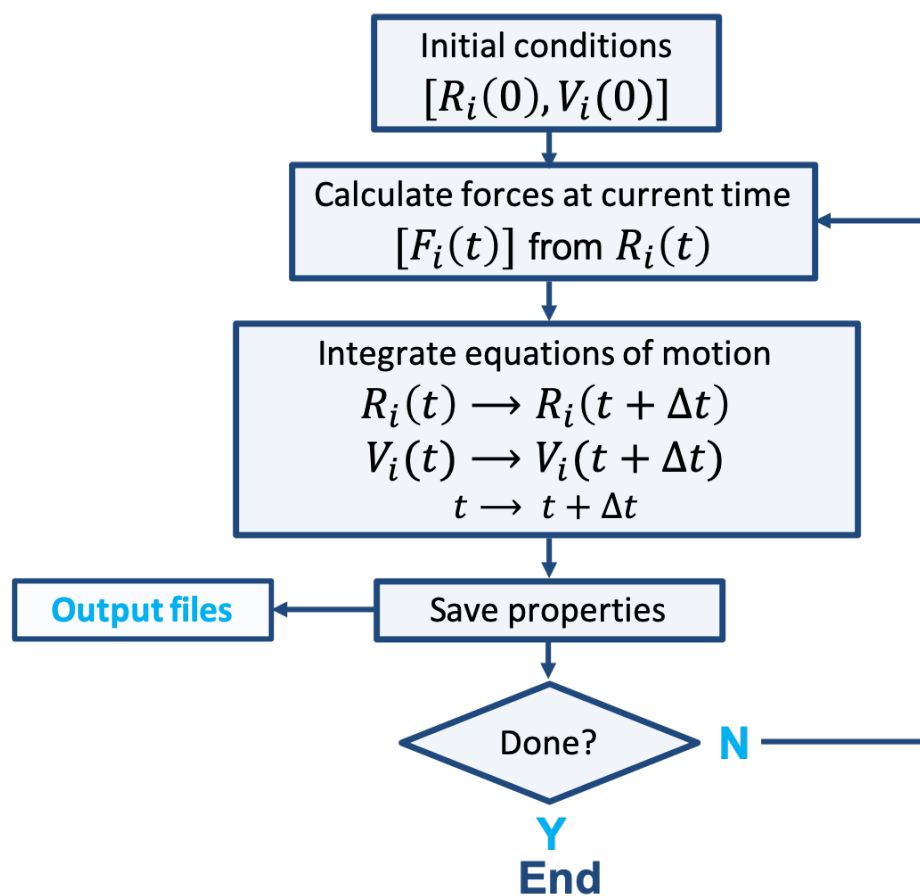


Figure 2.1.: Structure of a minimalist molecular dynamics code. Reproduced from “From Atoms to Materials: Predictive Theory and Simulations” [53]

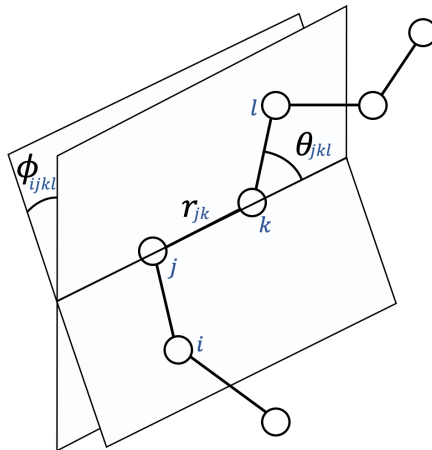


Figure 2.2.: Schematic of a simple chain molecule including bond r , bend angle θ and torsion angle ϕ . Reproduced from “Introduction to Molecular Dynamics Simulation”

Bonded Interactions In molecular systems we have to consider intramolecular bonding interactions such as bend angle and torsion angle to give accurate description of the structures. A simple model of a polymer chain will include bond r_{ij} , angle θ_{jkl} and torsion ϕ_{ijkl} terms as displayed in Figure 2.2.

- (1) DREIDING is a all-purpose force field based on simple hybridization rules with harmonic valence terms for bond stretching and bend angle, and a cosine-Fourier expansion for the torsion term as show in Equation 2.6. In consequence it has good coverage for organic, biological and main-group inorganic molecules and it has been widely used in the prediction of thermoplastic polymers [58] and thermosets. [59]

$$\begin{aligned}
 v^{\text{bonded}} = & \frac{1}{2} \sum_r k^r (r - r_0)^2 + \frac{1}{2} \sum_\theta k^\theta (\theta - \theta_0)^2 \\
 & + \frac{1}{2} \sum_\phi k^{\phi,n} [1 - \cos(n\phi - \gamma_n)] + \frac{1}{2} \sum_\psi k^\psi (\cos \psi - \cos \psi_0)^2
 \end{aligned} \tag{2.6}$$

- (2) PCFF belongs to the second-generation consistent force fields, characterized by their ability of predicting many properties in a broad range of polymers and organic materials. It employs quartic polynomials for bond stretching and angle bending, a three-

term Fourier expansion for torsions, and many cross-terms: bond-bond, bond-angle, angle-angle, bond-torsion, angle-torsion, and angle- angle-torsion.

$$\begin{aligned}
v^{\text{bonded}} = & \sum_{r,n=2}^4 k^{r,n} (r - r_0)^n + \sum_{\theta,n=2}^4 k^{\theta,n} (\theta - \theta_0)^n \\
& + \sum_{\phi,n=1}^3 k^{\phi,n} [1 - \cos(n\phi - \gamma_n)] + \sum_{\psi} k^{\psi} (\psi - \psi_0)^2 \\
& + \sum_{rr'} k(r - r_0)(r' - r'_0) + \sum_{\theta\theta'} k(\theta - \theta_0)(\theta' - \theta'_0) + \sum_{r\theta} k(r - r_0)(\theta - \theta_0) \quad (2.7) \\
& + \sum_{r\phi} \left[k(r - r_0) \sum_{n=1}^3 k^{r\phi,n} \cos n\phi \right] + \sum_{\theta\phi} \left[k(\theta - \theta_0) \sum_{n=1}^3 k^n \cos n\phi \right] \\
& + \sum_{\theta\theta\phi} k(\theta - \theta_0)(\theta' - \theta'_0) \cos \phi
\end{aligned}$$

Non-bonded Interactions The non-bonded terms are usually split in 2-body, 3-body and/or 4-body terms. In simulations of polymeric materials is usual to concentrate on the pair potential $v(r_i, r_j) = v(r_{ij})$, known as van der Waals interactions. A simple model for non-bonded terms uses Lennard-Jones (LJ) potential,

$$v^{\text{LJ}}(r) = 4\epsilon \left[\left(\frac{\sigma}{r} \right)^{12} - \left(\frac{\sigma}{r} \right)^6 \right] \quad (2.8)$$

We should point out that the PCFF force field uses a LJ potential but using the 9-3 form: $\epsilon \left[2 \left(\frac{\sigma}{r} \right)^9 - 3 \left(\frac{\sigma}{r} \right)^6 \right]$. Although DREIDING allows non-bonded interactions to be described as LJ, a more common choice, and the one used along the majority of the work is proposed by Buckingham, [60]

$$v^{\text{B}}(r) = Ae^{-Br} - \frac{C}{r^6} \quad (2.9)$$

where A, B, C > 0. If electrostatic charges are present, Coulomb potentials are added on the form:

$$v^{\text{Coulomb}}(r) = \frac{Q_1 Q_2}{4\pi\epsilon_0 r} \quad (2.10)$$

2.2 Setting Up a Molecular Dynamics Simulation

In the previous section, a brief description of how a classical MD simulation works is given. However, we have not mentioned that before running simulation it is not only required to pick a force field and prepare information indispensable, but also it is mandatory to set up the atomic or molecular structure of interest. Depending on the system, different methodologies are used to create the initial structure, in some cases the MD engine by itself can do this task.

Since we focus in this work in organic and polymeric materials, we want to highlight some approaches to generate the structure to be read by the MD simulator.

2.2.1 Structure to LAMMPS

In some cases, it is usual to have available a molecular or crystal structure, consisting of the atomic coordinates but no connectivity or force field in the format read by LAMMPS. For that reason, we have created a tool, [LAMMPS Data File Generator](#) [61], capable of generating a data file for the structure of interest with all the required information to perform simulations with the DREIDING force field.

The tool framework involves several procedures that can be summarized in four steps as shown in Figure 2.3. First, the tool reads a structure in a broad list of formats, and uses OpenBabel [62] and Ovito [63] to convert it into a data file format that can be used in LAMMPS. After successful conversion of the file, we proceed with a set of scripts written in Python in order to find the full connectivity: bonds, angles, dihedrals and impropers, integrating LAMMPS for this task. The third step consists in assigning all the force field parameters including the correct atom types and energy terms. In this step the atomic charges are also calculated. Lastly, we gather all the information to generate the data file in the proper format.

One of the key features of the tool is the flexibility to read multiple file formats. This can be problematic sometimes since the simulation cell is not specified or it is incorrect as the one expected from the user. In order to consider this, the tool allows to control the

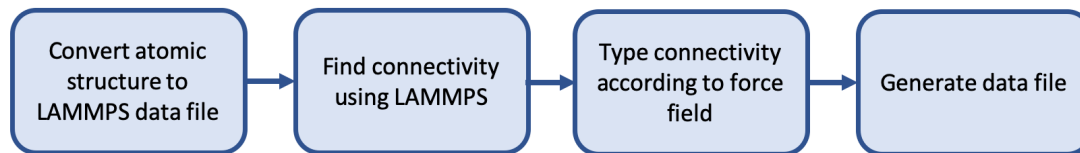


Figure 2.3.: Schematic of the methodology implemented in the LAMMPS Data File Generator tool

simulation cell information. The user can eventually input the box lengths and angles. In Figure 2.4 a snapshot of the tool is displayed. After file upload, the user can visualize the structure to be converted and input any additional information, regarding simulation cell. After clicking *Create Data File* output details are given, once it is done, users can download the file.

LAMMPS Data File Generator

This tool generates all necessary input files for LAMMPS simulations of molecular systems starting with an atomistic structure.

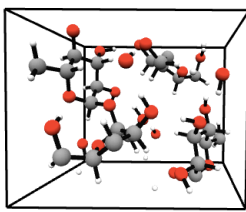
Tool features:

- Accepts a wide range of input formats (e.g. CIF, PDB, XYZ)
- Works with periodic boundary conditions, even when covalent bonds cross boundariesThe tool uses OpenBabel to convert the initial files
- Sets up energy expression for Dreiding and PCFF force fields (including automatic bond recognition and atom typing)
- Assigns atomic charges using the Gasteiger method

Known bug: If resonance ring crosses the boundary, atoms will be incorrectly typed

1) Upload File in any [format supported by OpenBabel](#).

File uploaded successfully



2) Additional inputs

☒ Simulation box included in file

x: α :
 y: β :
 z: γ :

Force field:
 Bonds scale:
 Charge:

Note: Simulation cell parameters [Å]

Creating bonds ...

Box size parameters read:
 x: 0.000 7.832
 y: 0.000 8.800
 z: 0.000 10.407
 -3.8466024e-07 -2.4658308 -5.7527819e-07 xy xz yz

Number of atoms: 90
 Number of bonds: 92
 Bonds have been identified
 90
 Getting information...
 Generating DREIDING atom types
 Equilibrating charge...

Total charge= 1.22124532709e-15
 LAMMPSDataFile.data created!

Figure 2.4.: Snapshot of the LAMMPS Data File Generator tool, available in [nanoHUB](#). The tool can be used to convert atomic and molecular structures into a LAMMPS data file containing all the connectivity and force field terms required to run a MD simulation

2.2.2 Building a Structure

In some scenarios, like in polymers, it is necessary to build a sample from a repeating unit such as a monomer. To do so, several software have been developed and most of them integrate a force field to avoid bad contacts during the polymerization procedure and to allow performing simulations. We will give a description of Polymer Modeler [64], available for freely at [nanoHUB](#), a tool in which users can build polymeric systems and get a data file ready to perform MD simulations in LAMMPS using the DREIDING force field.

Polymer Modeler The polymer builder tool allows the user to create atomic level structures of linear polymer chains from a monomer. The process of building is made up of three steps: (i) monomer(s) specification, chain length and number of chains, (ii) simulation cell, (iii) placement of monomers and conformation given by dihedral angles; this is done using the configurational bias Monte Carlo Algorithm. However, other chain builder choices are available in the tool, alongside with multiple inputs that the user can modify, such as the temperature to generate the sample, and furthermore, it allows to relax and perform MD simulations with the structure generated. More details about the tool and the methodology implemented can be found in Ref. [65].

3. UNCERTAINTIES IN PREDICTED THERMO-PHYSICAL PROPERTIES OF THERMOPLASTIC POLYMERS USING MOLECULAR DYNAMICS

ADAPTED FROM:

Lorena Alzate-Vargas et al. 2017 Uncertainties of Parameters to Predictions of Polymer Properties by Molecular Simulations. Proceedings of the American Society for Composites © 2017 DEStech Publications, Inc. and American Society for Composites

Lorena Alzate-Vargas et al. 2018 Modelling and Simulation in Materials Science and Engineering, **26**, 065007 © 2018 IOP Publishing Ltd.

3.1 Introduction

Quantification of such uncertainties in models as well as in experiments is a critical step in model validation. [8] Specially, if tools are to be used in decision making.

The computational materials discovery or optimization involving properties that depend on processing, microstructure or molecular structure is significantly more complex since the coupling of various models is often needed to describe structure and properties, see for example Ref. [66]. It is often the case that uncertainties in these models are poorly understood and can vary significantly from material to material and from property to property.

The validation of a model is not trivial due to different sources of uncertainties that can affect both modeling and experimental results.

Uncertainties that can result in discrepancies between experiments and simulation originate from a variety of sources: (i) Fundamental limitations of the underlying models such as the choice of exchange and correlation functional in density functional theory or inter-atomic potentials in molecular dynamics (MD). (ii) Differences in the material modeled and that characterized experimentally; e.g. simplification of the molecular structure of polymers or

neglect of defects and microstructure in the simulation. (iii) Differences in the testing procedures between experiments and simulations; e.g. ultra-fast deformation or heating/cooling in MD simulations. (iv) Data analysis. In the latter one, both in simulations and experiments, it is often the case that the quantity of interest is not measured directly but extracted through the application of data analysis techniques and/or use of models.

In this work we focus on assessing the uncertainties introduced in the prediction of some important thermo-physical properties of two well known polymers.

We use state-of-the-art molecular simulations to assess the uncertainties associated in glass transition temperature T_g , density ρ at 300 K, and coefficient of thermal expansion α_V for two thermoplastic polymers: poly(methyl-methacrylate) (PMMA) and polystyrene (PS). We independently quantify how the predictions are affected by the various sources of uncertainties in the simulations, which include: (i) the method used to generate the initial amorphous structures, (ii) the molecular weight of the samples, (iii) the force field used to describe atomic interactions, (iv) the analysis used to extract the quantities of interest.

We find that the simulations can capture subtle differences in T_g and density between these two polymers and that all sources of uncertainties studied affect predictions, but their relative importance depends on the specific quantity of interest. As expected, the choice of force fields affects the predicted quantities and our analysis provides insight into the molecular origins of these differences. Data analysis affects in an important way certain properties, particularly T_g in our study. Our results indicate significant care should be devoted to this aspect of the simulation workflow. Finally, the polymer builder influences the molecular structure and therefore the properties; interestingly, the effect of the builders used on predicted properties cannot be explained via different thermal histories of the structures generated with different builders.

Work published in Proceedings of the American Society for Composites 2017 and Modelling and Simulation in Modelling and Simulation in Materials Science and Engineering with Chunyu Li, Benjamin Haley, Michael Fortunato, Coray Colina, and Alejandro Strachan as coauthors [67, 68]

3.2 Simulation Details

3.2.1 Molecular Systems

Several molecular models of PMMA and PS were built and used as initial conditions for MD simulations to extract the desired properties. For each polymer we studied two different molecular architectures to assess the effect of chain molecular weight: (1) 10 chains, 70 repeating units and, (2) 1 chain, 700 repeating units. The total number of atoms in each simulation was 10,520 and 10,502 for PMMA and 11,220 and 11,202 for PS. These systems were chosen to have a similar number of atoms and are comparable to or larger than those typically used in MD studies of soft materials.

A full schematic of the methodology implemented in this work is shown in Figure 3.1. More details for every step are given below.

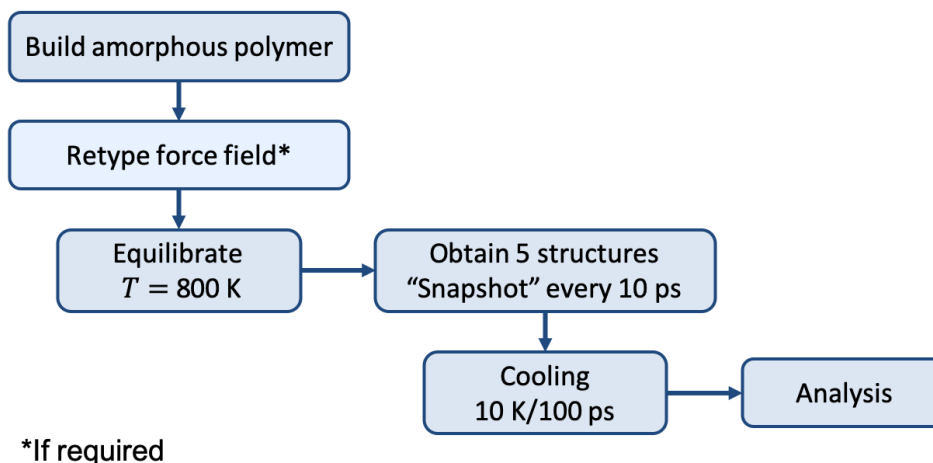


Figure 3.1.: Schematic of the methodology implemented in the present work

One of the first decisions to be made in a molecular simulation is the force field to describe the interactions. It must be said that a proper choice can lead to good prediction of macroscopic properties. In this work we compare predictions for two widely used force fields: DREIDING and PCFF; their description can be found in section 2.1.3.

In order to minimize variability in predictions associated with electrostatic interactions,

we used the same partial atomic charges obtained using the Gasteiger method [69] for all simulations.

3.2.2 Amorphous Structure Generation

We used two different approaches to prepare the molecular structures of the polymers: continuous configurational bias Monte Carlo as implemented in the Polymer Modeler tool and described in 2.2.2 and self-avoiding random walk implemented in pysimm. [70]

Continuous Configurational Bias Monte Carlo In the CBMC method the sequential chain growth follows a Monte Carlo algorithm including the probability of chain conformations based on a Boltzmann distribution of torsion energies along the backbone atoms along with non-bond interactions followed by an equilibration.

During the building procedure the bond distances and angles are fixed at equilibrium so the dihedral angles are the only available degree of freedom.

Polymers were built at an initial density of 0.5 g/cm^3 and temperature $T = 300 \text{ K}$ for PMMA and $T = 800 \text{ K}$ for PS using the DREIDING force field parameters. A higher temperature for PS was chosen due to its more rigid side chains relaxing faster in the liquid state.

The relaxation procedure consisted of a 3-level step energy minimization with scaled van der Waals parameters; followed by an MD simulation under the NVT ensemble for 50 ps, and a second simulation under NPT conditions for 100 ps. After equilibration, the systems were re-typed to PCFF.

Self-Avoiding Random Walk The SARW method inserts reference monomer units sequentially at chain ends, introducing one new polymer bond per insertion, to grow a polymer chain with the desired length. Monomer insertion will not be at the optimal position and the algorithm allows the structure to relax using energy minimization during the building procedure.

The polymer structure is originally built using the Generalized Amber Force Field (GAFF) but force field parameters were switched to PCFF before the system was equilibrated. Structures are created at low density of 0.3 g/cm^3 and subsequently equilibrated using a compression/relaxation scheme of MD simulations with varying temperature and pressure [70].

The MD equilibration procedure consist in the seven repetitions of the following cycle:

- an NVT simulation at $T_{\text{high}} = 1000 \text{ K}$,
- a second NVT simulation at $T_{\text{final}} = 600 \text{ K}$,
- and a NPT simulation at T_{final}

The pressure during each cycle varied step wise to reach $P_{\text{max}} = 50000 \text{ atm}$ and then to $P_{\text{final}} = 1 \text{ atm}$. The length of each simulation was 50 ps.

We used the SARW method to generate PMMA samples, therefore no PS data will be presented with this builder.

Since both builders use force fields to avoid bad contacts during the chain growth process and to relax structures. In order separate the build process and the MD simulations used to extract the quantities of interests (for short notation as QoIs) and quantify separate uncertainties, the force field adapted in the builder does not match the one used in the predictions. Thus, the initial structures used for DREIDING and PCFF predictions are identical.

3.2.3 Molecular Dynamics Simulations

Each polymer structure obtained according to the combination of molecular weight, builder, and force field was subject to the same MD simulation performed using LAMMPS. [71] For all systems, non-bonded long-range electrostatic interactions were described using the particle-particle, particle-mesh method with a precision of $10^{-4} \text{ kcal/mol.Å}$. A time step of 1 fs was used in all the simulations. These choices lead to good energy conservation under NVE conditions.

Initial Structure Thermalization Before performing the simulations designed to extract the quantities of interest, we thermalized the structures obtained from the two amorphous builders and took them to a temperature of 800 K. This equilibration was performed under constant temperature and pressure of 1 atm for 500 ps using a Nose-Hoover thermostat and barostat. In all simulations the barostat maintained the shape of the simulation cell fixed (cell parameters are scaled by the same amount) and we used relaxation timescales of 0.1 ps for the thermostat and 1 ps for the barostat.

For each molecular weight, builder, and force field we obtained five independent structures from an additional 50 ps of simulation at 800 K; each structure separated from the next by 10 ps of MD simulation. While 10 ps at 800 K is enough to de-correlate the initial structures and enables us to have better statistics, this time (even including the prior thermalization) is not enough for the molecular chain structure to evolve significantly, thus, we expect that the predictions will depend on the builder used to generate the initial structures.

Cooling In order to extract the desired quantities of interest, each one of the 40 simulations was cooled in a step wise manner at constant pressure of 1 atm to $T_{\text{final}} = 100$ K. The temperature is decreased every 100 ps in steps of 10 K.

3.2.4 Data Analysis procedure

One of the sources of uncertainty in MD simulations that has been vaguely explored is the procedure to extract properties from raw data. Because of the quantities of interest in this work, we used the density versus temperature (ρ vs. T) MD data. Two fitting methods based on the Levenberg-Marquardt algorithm [72] implemented in the [scipy.optimize.leastsq](#) library in Python, are programmed in order to extract the various QoIs. A representation of each method is shown in Fig. 3.7.

Bilinear fit This is the most commonly used procedure to determine the glass transition temperature. It consists in fitting two straight lines: one the low temperature regime and one for the high temperature regime. The intersection between them, where a change

in the slope occurs will be denote T_g . The volumetric coefficients of thermal expansion (above and below T_g) were extracted from the slopes of each fitted line by converting the density to volumetric data.

Hyperbola fit This procedure consists in fitting a hyperbola to the density vs. temperature data, as done in Ref. [12]. The asymptotes of the hyperbola denote the low and high temperature regimes and the intersection between them defines the glass transition temperature.

Since we have five configurations for each scenario, we implemented two averaging procedures: (i) analyze each individual sample to obtain the quantities of interest followed by an average of the results, for short notation QoI Ave and, (ii) average the MD data for the density and temperature over the five samples and perform the analysis, referred as MD Ave.

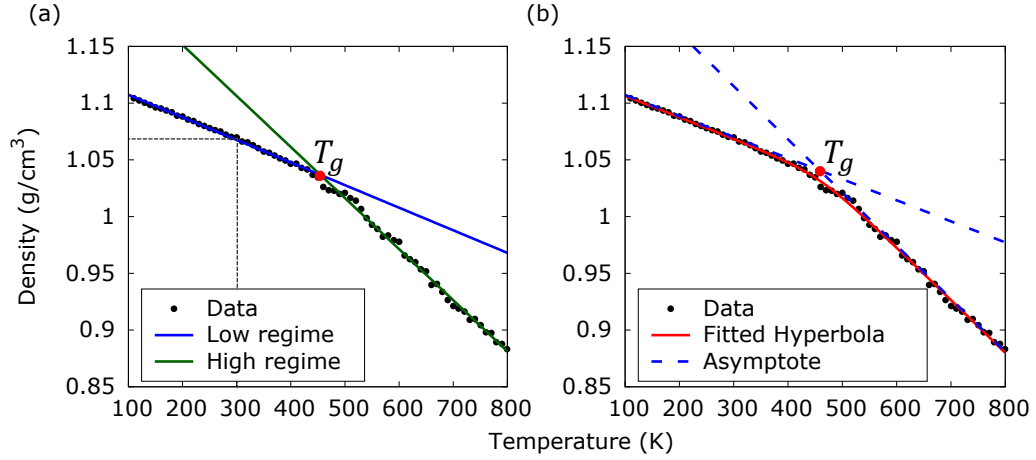


Figure 3.2.: Estimates of T_g (red point) from a single simulation using two fitting procedures: (a) T_g is estimated as the intersection of low (blue) and high (green) temperature best-fit lines and (b) Hyperbola (red) fit to the data, here T_g is estimated from the intersection of the asymptotes (dashed blue)

Confidence intervals We have consistently reported the 90% confidence intervals for the predicted QoIs calculated as

$$t_{(\alpha/2)} \sqrt{\left(\frac{\sigma^2}{n}\right)} \quad (3.1)$$

where $t_{(\alpha/2)} = 1.645$ is the t -value from the standard normal distribution for the selected confidence percentage and σ/\sqrt{n} the standard error of the mean. [73] σ is the standard deviation of the density data for the five runs and $n = 500$ is the number of independent density points from the five simulations.

The confidence intervals for T_g and α_V are obtained from the fitting procedure as $t^* \cdot \text{SE}$, where SE is the standard error and $t^* = 1.6683$ from the Student t -distribution (data points minus number of parameters fitted). [74]

3.2.5 Conformational transition analysis

To explain the trends observed, we have characterized the local chain dynamics by means of the conformational transition rates in torsional angles along the chain backbone. There is a general consensus that a dihedral angle undergoes a transition when it rotates enough to reach a new configurational stage in the potential well. [46, 75, 76] Following the same definition, we monitor the time evolution of a torsion from the trajectory of the atoms obtained in MD, spaced every 4 ps. A transition has occurred at t_i if

$$\left. \begin{array}{l} \Delta\phi[(t_i + 4 \text{ ps}) - (t_i - 4 \text{ ps})] \\ \text{and} \\ \Delta\phi[(t_i + 8 \text{ ps}) - (t_i - 8 \text{ ps})] \end{array} \right\} \geq 80^\circ$$

This procedure of analyzing a range of 16 ps was designed to count states with residence times longer than a few torsional vibrational periods. Torsional transition rate k at a given temperature is defined as:

$$k = \frac{N_{\text{tr}}}{N_\phi t} \quad (3.2)$$

where N_{tr} is the total number of transitions during the run, N_{ϕ} is the total backbone torsions in the system, and t the total simulation time.

3.3 Predictions and Comparison Against Experiments

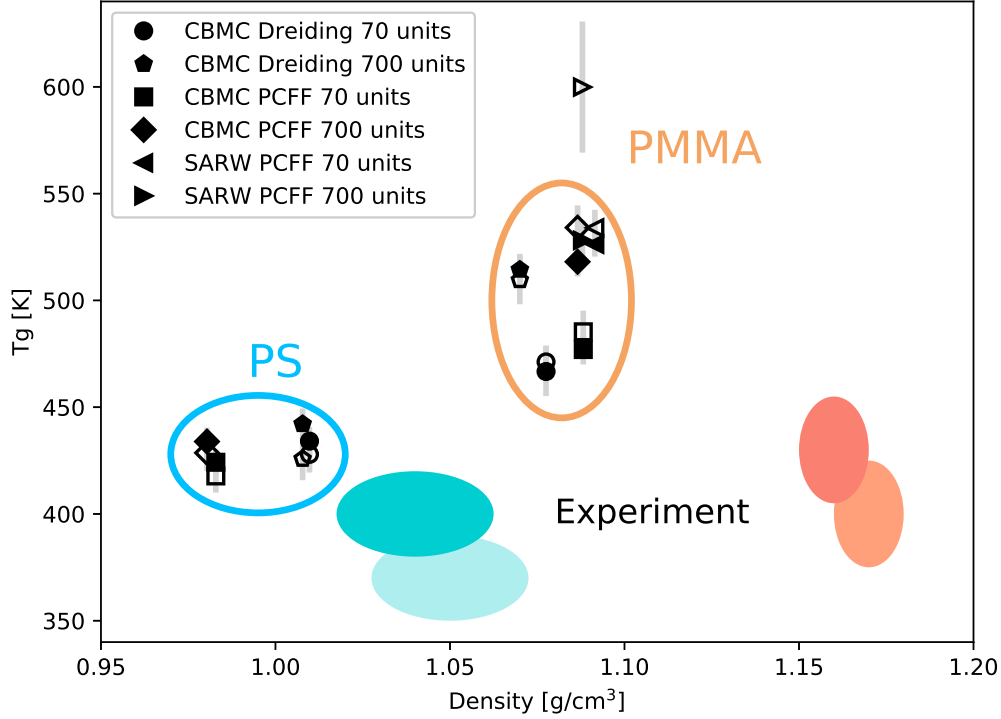


Figure 3.3.: Glass transition T_g (MD Ave) and density at 300 K for different input choices. Filled symbols represent predicted values using bilinear fitting method, empty symbols represent values obtained with the hyperbola method. Predictions are circled in orange for PMMA and blue for PS, light colored ellipses refer to experimental data whereas dark colored ellipses represent WLF-corrected experimental data.

Figure 3.3 compares the predicted T_g (each symbol represents a combination) and densities at 300 K with their respective confidence intervals, together with experimental data for PS and PMMA (large light-colored ovals). The densities shown in Fig. 3.3 represent the average density ($\bar{\rho}$) extracted from the last 50 ps of the MD simulations at 300 K for the five independent runs and MD Ave T_g obtained from the two fitting procedures. Error bars represent 90% confidence intervals as discussed in section 3.2.4.

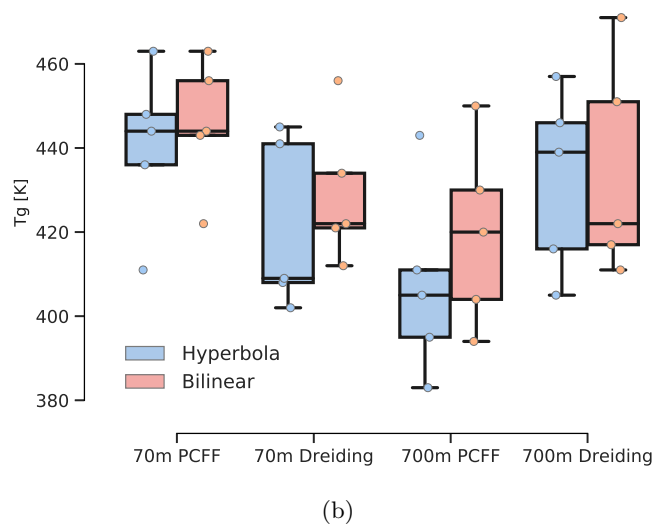
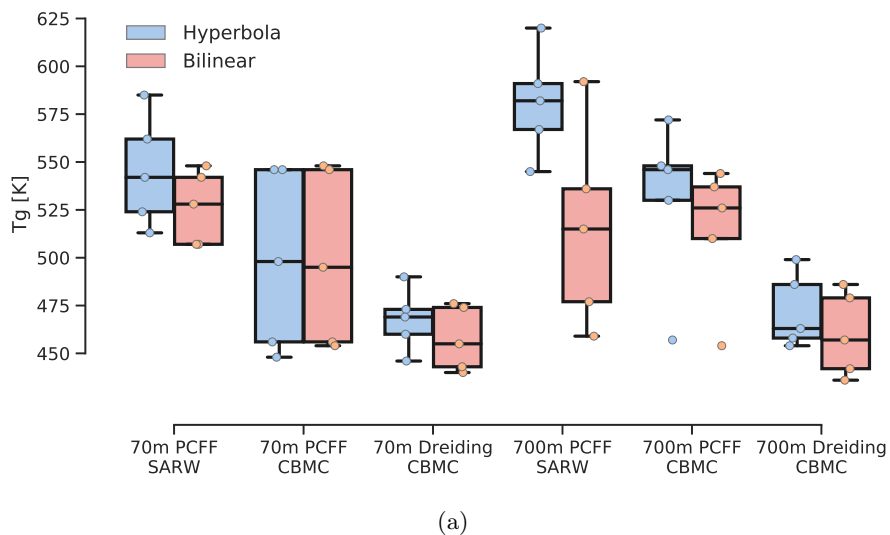


Figure 3.4.: Predicted glass transition temperatures for each combination of input choices in polymer samples (a) PMMA and (b) PS. All PS simulations are performed by generating samples with the same amorphous builder method

The MD simulations resulted in higher glass transition temperatures and lower densities as compared with experiments. This is as expected since the cooling rates used in the simulations are approximately 12 orders of magnitude faster than the experimental rates. The effect of cooling rate on T_g can be estimated using the Williams-Landau-Ferry (WLF) theory [77] that describes relaxation processes in polymers and organic liquids.

The WLF equation predicts an increase in T_g of approximately 3 K to 5 K per order of magnitude in heating or cooling rate. [78, 79] The raise in T_g is accompanied by a decrease in density of $\Delta T_g(\alpha_{\text{glass}} - \alpha_{\text{liq}})$, [80] where α_{glass} is the slope of the density-temperature data below T_g and α_{liq} is the slope above T_g . We also include these WLF-modified experimental values, using a conservative choice of 3 K increase in T_g per order or magnitude, as darker areas in Fig. 3.3. Larger values for shifting T_g according to cooling rate would result in better agreement between the simulations and experiments.

The presented results show that the simulations not only can capture the increase in density and T_g going from PS to PMMA, but the predicted values are very close to the experimental ones. We note that the discrepancy between simulations and experiments is larger for PMMA than PS, understanding the origin of this observation is beyond the scope of this work but a possible reason could be the large ionic character of PMMA.

The distribution of predicted T_g s with respect to every choice-combination is shown in Figure 3.4. We can see the large variability that arises from the data analysis in several combinations for each dataset consisting of five configurations. To consistently summarize all the predictions from our simulations, including error analysis, Tables 3.1 and 3.2 are included in this document. Along with Fig. 3.4, they show clear differences between predicted QoI with respect to the various simulation and data analysis choices; these will be discussed in the following section. Predicted values for α_V convey in good agreement with experimental data. [81]

As a reminder, the density at 300 K was obtained directly from the MD raw output and consequently there is not distinction between the bilinear and hyperbola analysis.

Table 3.1.
Predicted densities at room temperature, glass transition temperatures and coefficient of thermal expansion for poly(methyl-metacrylate) systems

| | 70 monomers | | | | | | 700 monomers | | | | | |
|---|-------------|-------|---------|-------|----------|-------|--------------|-------|---------|-------|----------|-------|
| | SARW | | CBMC | | | | SARW | | CBMC | | | |
| | PCFF | | PCFF | | DREIDING | | PCFF | | PCFF | | DREIDING | |
| | H | B | H | B | H | B | H | B | H | B | H | B |
| $\bar{\rho}$ [g/cm ³] | 1.092 | | 1.088 | | 1.078 | | 1.088 | | 1.087 | | 1.070 | |
| σ | 0.00341 | | 0.00363 | | 0.00956 | | 0.00609 | | 0.00658 | | 0.00466 | |
| $t_{\alpha/2} \cdot \sigma / \sqrt{n}$ | 0.00025 | | 0.00027 | | 0.0007 | | 0.00045 | | 0.00048 | | 0.00034 | |
| T_g (MD Ave) [K] | 534 | 526 | 485 | 477 | 471 | 467 | 600 | 528 | 534 | 518 | 509 | 514 |
| Std Error | 5.1 | 3.5 | 5.9 | 4.2 | 4.6 | 6.9 | 18.3 | 5.6 | 6.2 | 4.1 | 6.8 | 4.4 |
| $t^* \cdot \text{SE}$ | 8.43 | 5.84 | 9.9 | 7.04 | 7.72 | 11.51 | 30.6 | 9.26 | 10.4 | 6.9 | 11.3 | 7.36 |
| T_g (Qol Ave) [K] | 545 | 526 | 499 | 500 | 470 | 462 | 581 | 516 | 531 | 514 | 514 | 515 |
| $\sigma / \sqrt{5}$ | 11.6 | 7.66 | 18.84 | 18.47 | 16.46 | 12.2 | 11.6 | 20.93 | 17.5 | 14.4 | 11.34 | 11.1 |
| $t_{\alpha/2} \cdot \sigma / \sqrt{5}$ | 19.07 | 12.6 | 30.9 | 30.38 | 27.07 | 20.17 | 18.36 | 34.42 | 28.8 | 23.7 | 20.8 | 18.26 |
| α_V^- (MD Ave) [$\times 10^{-4}$ K ⁻¹] | 2.42 | 2.07 | 2.26 | 1.92 | 2.37 | 2.08 | 2.35 | 2.03 | 2.21 | 1.9 | 2.19 | 1.95 |
| Std Error [$\times 10^{-4}$ K ⁻¹] | 0.043 | 0.026 | 0.067 | 0.032 | 0.016 | 0.063 | 0.163 | 0.035 | 0.054 | 0.026 | 0.09 | 0.37 |
| $t^* \cdot \text{SE}$ [$\times 10^{-4}$ K ⁻¹] | 0.072 | 0.044 | 0.113 | 0.053 | 0.266 | 0.105 | 0.272 | 0.058 | 0.089 | 0.044 | 0.15 | 0.62 |
| α_V^- (Qol Ave) [$\times 10^{-4}$ K ⁻¹] | 2.42 | 2.06 | 2.29 | 19.5 | 2.27 | 2.07 | 2.29 | 2.01 | 2.19 | 1.89 | 2.14 | 1.96 |
| $\sigma / \sqrt{5}$ [$\times 10^{-4}$ K ⁻¹] | 0.046 | 0.038 | 0.07 | 0.054 | 0.045 | 0.038 | 0.033 | 0.032 | 0.023 | 0.014 | 0.068 | 0.05 |
| $t_{\alpha/2} \cdot \sigma / \sqrt{5}$ [$\times 10^{-4}$ K ⁻¹] | 0.075 | 0.062 | 0.115 | 0.089 | 0.074 | 0.062 | 0.054 | 0.052 | 0.038 | 0.022 | 0.111 | 0.083 |
| α_V^+ (MD Ave) [$\times 10^{-4}$ K ⁻¹] | 4.85 | 5.09 | 4.18 | 4.31 | 5.58 | 6.25 | 4.41 | 4.63 | 4.21 | 4.35 | 5.13 | 5.65 |
| Std Error [$\times 10^{-4}$ K ⁻¹] | 0.161 | 0.055 | 0.067 | 0.043 | 0.37 | 0.85 | 0.52 | 0.072 | 0.186 | 0.05 | 0.27 | 0.07 |
| $t^* \cdot \text{SE}$ [$\times 10^{-4}$ K ⁻¹] | 0.268 | 0.091 | 0.113 | 0.071 | 0.618 | 0.142 | 0.872 | 0.12 | 0.311 | 0.083 | 0.463 | 0.117 |
| α_V^+ (Qol Ave) [$\times 10^{-4}$ K ⁻¹] | 4.3 | 4.93 | 4.28 | 4.96 | 5.6 | 6.28 | 4.32 | 4.65 | 4.22 | 4.37 | 5.14 | 5.73 |
| $\sigma / \sqrt{5}$ [$\times 10^{-4}$ K ⁻¹] | 0.096 | 0.182 | 0.36 | 0.36 | 0.07 | 0.046 | 0.074 | 0.115 | 0.158 | 0.178 | 0.072 | 0.112 |
| $t_{\alpha/2} \cdot \sigma / \sqrt{5}$ [$\times 10^{-4}$ K ⁻¹] | 0.158 | 0.3 | 0.591 | 0.591 | 0.115 | 0.076 | 0.121 | 0.188 | 0.26 | 0.293 | 0.118 | 0.184 |

For short notation hyperbola fitting is referred as H and bilinear fitting as B

Table 3.2.

Predicted densities at room temperature, glass transition temperatures and coefficient of thermal expansion for polystyrene systems

| | 70 monomers | | | | 700 monomers | | | |
|---|-------------|-------|----------|-------|--------------|-------|----------|-------|
| | PCFF | | DREIDING | | PCFF | | DREIDING | |
| | H | B | H | B | H | B | H | B |
| $\bar{\rho}$ [g/cm ³] | 0.983 | | 1.010 | | 0.980 | | 1.008 | |
| σ | 0.00391 | | 0.00475 | | 0.00477 | | 0.00436 | |
| $t_{\alpha/2} \cdot \sigma / \sqrt{n}$ | 0.00029 | | 0.00035 | | 0.00035 | | 0.00032 | |
| T_g (MD Ave) [K] | 418 | 424 | 428 | 434 | 429 | 434 | 426 | 442 |
| Std Error | 4.7 | 3.6 | 5.1 | 3.9 | 5.0 | 3.9 | 6.0 | 4.4 |
| $t^* \cdot \text{SE}$ | 7.8 | 5.9 | 8.5 | 6.6 | 8.4 | 6.5 | 10.02 | 7.27 |
| T_g (Qol Ave) [K] | 421 | 429 | 428 | 438 | 433 | 434 | 426 | 439 |
| $\sigma / \sqrt{5}$ | 8.1 | 6.8 | 4.94 | 6.42 | 8.61 | 9.34 | 8.34 | 5.64 |
| $t_{\alpha/2} \cdot \sigma / \sqrt{5}$ | 13.36 | 11.2 | 8.13 | 10.57 | 14.16 | 15.37 | 13.73 | 9.28 |
| α_V^- (MD Ave) [$\times 10^{-4}$ K ⁻¹] | 2.71 | 2.63 | 2.43 | 2.46 | 2.8 | 2.73 | 2.39 | 2.40 |
| Std Error [$\times 10^{-4}$ K ⁻¹] | 0.082 | 0.058 | 0.087 | 0.044 | 0.067 | 0.043 | 0.15 | 0.053 |
| $t^* \cdot \text{SE}$ [$\times 10^{-4}$ K ⁻¹] | 0.137 | 0.096 | 0.145 | 0.073 | 0.111 | 0.072 | 0.25 | 0.089 |
| α_V^- (Qol Ave) [$\times 10^{-4}$ K ⁻¹] | 2.69 | 2.60 | 2.44 | 2.45 | 2.77 | 2.69 | 2.36 | 2.39 |
| $\sigma / \sqrt{5}$ [$\times 10^{-4}$ K ⁻¹] | 0.061 | 0.057 | 0.06 | 0.069 | 0.07 | 0.066 | 0.022 | 0.021 |
| $t_{\alpha/2} \cdot \sigma / \sqrt{5}$ [$\times 10^{-4}$ K ⁻¹] | 0.1 | 0.095 | 0.099 | 0.114 | 0.115 | 0.108 | 0.037 | 0.034 |
| α_V^+ (MD Ave) [$\times 10^{-4}$ K ⁻¹] | 4.66 | 6.43 | 4.71 | 6.06 | 4.49 | 6.45 | 4.62 | 5.93 |
| Std Error [$\times 10^{-4}$ K ⁻¹] | 0.155 | 0.058 | 0.176 | 0.049 | 0.134 | 0.049 | 0.269 | 0.06 |
| $t^* \cdot \text{SE}$ [$\times 10^{-4}$ K ⁻¹] | 0.258 | 0.096 | 0.294 | 0.083 | 0.224 | 0.082 | 0.449 | 0.101 |
| α_V^+ (Qol Ave) [$\times 10^{-4}$ K ⁻¹] | 4.68 | 6.45 | 4.73 | 6.06 | 4.4 | 6.2 | 4.6 | 5.93 |
| $\sigma / \sqrt{5}$ [$\times 10^{-4}$ K ⁻¹] | 0.029 | 0.053 | 0.05 | 0.046 | 0.021 | 0.055 | 0.019 | 0.029 |
| $t_{\alpha/2} \cdot \sigma / \sqrt{5}$ [$\times 10^{-4}$ K ⁻¹] | 0.048 | 0.087 | 0.082 | 0.075 | 0.034 | 0.09 | 0.032 | 0.049 |

For short notation hyperbola fitting is referred as H and bilinear fitting as B

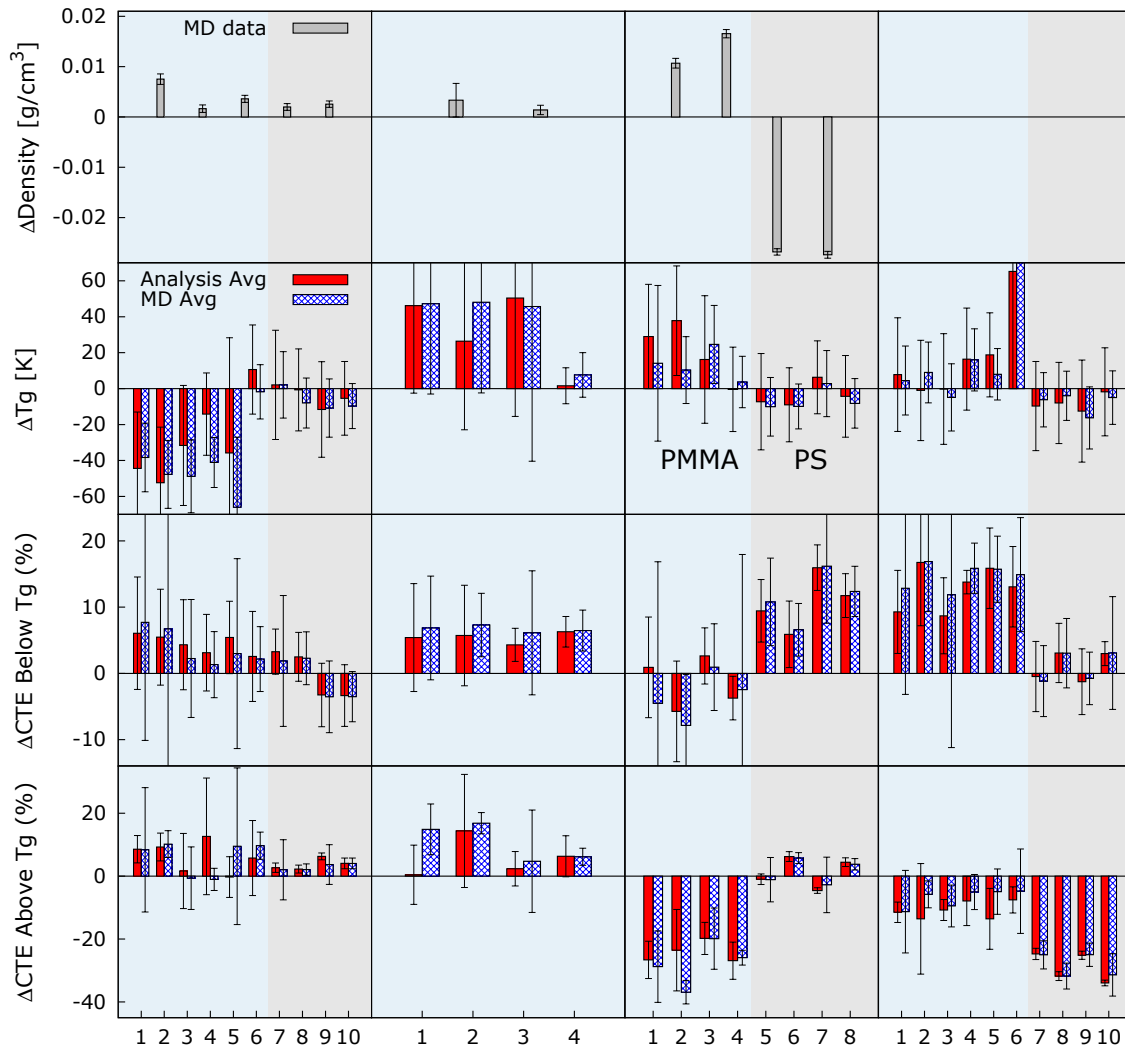
3.3.1 Role of Builder, Molecular Weight, Force Field and Data Analysis on Predicted Quantities

Figure 3.5 quantifies how each of the independent variables (organized in columns) affects the four QoIs (organized in rows) using raw results from Tables 3.1 and 3.2. The first column shows how molecular weight influences the QoIs; the bars represent the difference in prediction (results for systems composed of 70 monomers chains minus those for 700 monomers chain systems) and the various categories in the plot represent different combinations of the remaining independent variables.

For each case, we show the QoI Ave (solid red) and the MD Ave (hashed bars). The second column shows the effect of the builder (SARW - CBMC), the third force field (PCFF - DREIDING) and the forth column quantifies the effect of data analysis (hyperbola - bi-linear). Error bars represent the 90% confidence intervals of the two values subtracted as the square root of their sum of standard deviations. Our results indicate that all variables studied affect the predicted QoIs, but to different degrees. Comparing red (QoI Ave) and hashed (MD Ave) bars we find that the averaging procedure tends to have a relatively minor role.

Role of Molecular Weight. An increase in chain molecular weight is expected to result in an increase of T_g and density. [82] However, the molecular weight of the system with 1 chain, 700 monomers (70,084 g/mol for PMMA and 72,870 g/mol for PS) corresponds to a regime where T_g becomes independent of molecular weight. [83] Experimental results indicate that reducing the chain molecular weight to those corresponding to 70 monomers chains would lead to a reduction of T_g of approximately 5% for both polymers. This reduction is comparable with the level of accuracy of our calculations and was not observed in our simulations. As expected, the 70 monomers per chain systems exhibited higher α_V in the solid and liquid phases.

Role of Builder Amorphous polymer builders are known to be key for accurate predictions of amorphous polymers. This is due to the importance of the initial molecular



| Case | Chain length (70-700 monomers) | | | Builder (SARW-CBMC) | | | Force field (PCFF-Dreiding) | | | Method (Hyperbola-Bilinear) | | |
|------|-----------------------------------|----------|-----------|------------------------|------|-----------|--------------------------------|------|-----------|--------------------------------|------|----------|
| 1. | CBMC | Dreiding | Hyperbola | 70m | PCFF | Hyperbola | 70m | CBMC | Hyperbola | 70m | CBMC | Dreiding |
| 2. | CBMC | Dreiding | Bilinear | 70m | PCFF | Bilinear | 70m | CBMC | Bilinear | 70m | CBMC | PCFF |
| 3. | CBMC | PCFF | Hyperbola | 700m | PCFF | Hyperbola | 700m | CBMC | Hyperbola | 700m | CBMC | Dreiding |
| 4. | CBMC | PCFF | Bilinear | 700m | PCFF | Bilinear | 700m | CBMC | Bilinear | 700m | CBMC | PCFF |
| 5. | SARW | PCFF | Hyperbola | | | | 70m | CBMC | Hyperbola | 700m | SARW | PCFF |
| 6. | SARW | PCFF | Bilinear | | | | 70m | CBMC | Bilinear | 700m | SARW | PCFF |
| 7. | CBMC | Dreiding | Hyperbola | | | | 700m | CBMC | Hyperbola | 70m | CBMC | Dreiding |
| 8. | CBMC | Dreiding | Bilinear | | | | 700m | CBMC | Bilinear | 70m | CBMC | PCFF |
| 9. | CBMC | PCFF | Hyperbola | | | | 700m | CBMC | Dreiding | | | |
| 10. | CBMC | PCFF | Bilinear | | | | 700m | CBMC | PCFF | | | |

Figure 3.5.: Differences in predicted values for each of the quantities of interest originating from each of the independent variables studied. Red bars represent QoI Ave and hashed bars represent MD Ave

structure as the relaxation timescales of polymers with large molecular weight often exceed those achievable by MD, even in the liquid phase. [84, 85] Not surprisingly, the choice of amorphous builder affects the predicted QoIs. We found that the SARW method resulted in slightly higher density, T_g , and α_V s. While the differences between the two builders are comparable to the 90% confidence interval in many cases, they are observed relatively consistently for the systems with 70 monomers and the 700 monomer per chain. The higher coefficient of thermal expansion seen in the SARW structures indicate a faster degree of relaxation during cooling, which seems at odds with the higher room temperature density. This will be discussed further in section 3.4.

Role of Force Field As expected, the choice of force field has a relevant footprint on the predictions. We found that PCFF overestimates T_g and ρ in PMMA as compared to DREIDING while for PS, T_g calculations were similar in both force fields, but ρ was underestimated by PCFF. This shows a correlation between these properties, higher density corresponds to higher T_g across force fields. Interestingly, going from the glassy state to the liquid, DREIDING increased the α_V more than PCFF, this could be due to higher chain mobility seen in the first one, which will be explored further in section 3.4. In the glassy state, PCFF led to a higher α_V than DREIDING for PS indicating higher anharmonicities in the non-bond interactions.

Role of Data Analysis The functional form used to describe the density-temperature data leads to large uncertainties in the predicted T_g and α_V values. For T_g the uncertainties span between 5 K and 20 K and are comparable to the 90% confidence level, except one combination: SARW, PCFF, and 700 monomers; that exhibits higher uncertainties. Further analysis of this problematic case shows that the density vs. temperature data does not exhibit a clear break in slope, see Figure 3.6. Consequently, T_g is not well defined, as it has been pointed out by Patrone et al. (2016) since the transition region between low and high temperature regimes can occur over hundreds of degrees, it can be often difficult to identify the corresponding change in the slope and several attempts to extract T_g can give different

estimates.

This result shows that it is advantageous to utilize complementary tools to analyze the raw data. This is particularly important when the QoI is obtained from a non-trivial analysis such as identifying a change in slope. It is important to note, that even disregarding this specific case, the uncertainties associated with the predicted T_g introduced by the data analysis techniques are not negligible and of a magnitude comparable to the discrepancy between prediction and experiments.

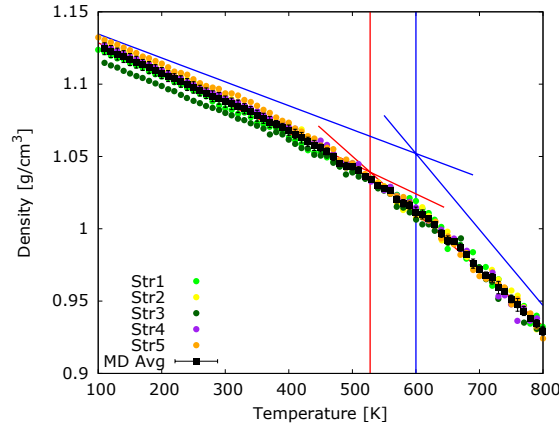


Figure 3.6.: Density vs temperature plot for combination: PMMA, 700 monomers, SARW, PCFF. This case results in a large variation for predicted T_g depending on the data analysis used. Predicted glass transition using bilinear fit shown in red and in blue for hyperbola fit method

The functional form used also affects the prediction of thermal expansion coefficient. Below T_g , the α_V obtained from the hyperbola fitting, evaluated at $T = 200$ K, is higher than the bilinear value (between 100K and T_g). Above T_g the hyperbola value, evaluated at $T = 700$ K, α_V is lower than the linear fit (between T_g and 800 K), this result relates to the fact that increasing the change in the temperature will increase the difference quotient (average slopes) of the function and therefore a high value is seen for the linear fit above T_g .

Effect of Temperature Range in Data Analysis On the other hand, we looked at the effect of the temperature range used in the regression model. We reduced the upper bound in the temperature regime to 700 K and 600 K and found significant variability on the predicted T_g as presented in Figure 3.7 for simulations done in PMMA.

An interesting response arises for the previously discussed case: SARW, PCFF, 700 monomers, denoted in the figure as PS700. The hyperbola based regression (hashed colored bars) can not find an estimate in the MD averaged data over the five samples if we exclude data points above 700 K. In contrast, a decrease in T_g is observed if the fit is performed between 100 K and 600 K.

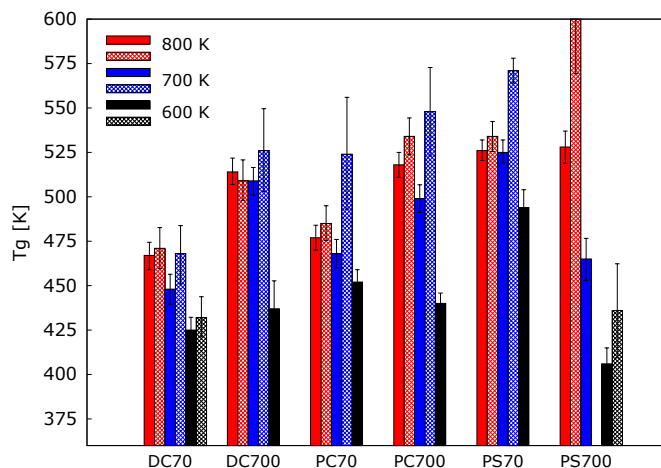


Figure 3.7.: Estimates of T_g for PMMA bulk samples with bilinear method (solid bars) and hyperbola method (hashed bars) according to the upper temperature regime used in the regression

3.4 Physical Origin of the Trends in Predictions

In order to understand the physical origin of the trends discussed in section 3.3.1, specifically, those associated with the choice of builder and force field, we analyzed the MD trajectories to quantify molecular processes responsible for the physical responses.

3.4.1 Amorphous builder

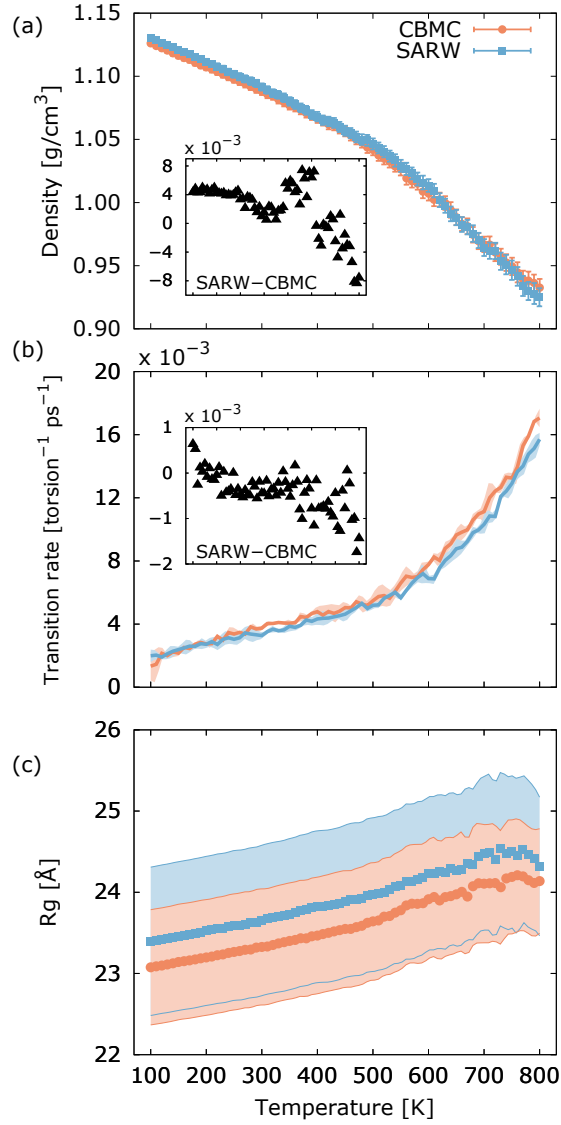


Figure 3.8.: Comparison of predicted properties within the two builders in PMMA systems with 70 monomers. (a) Density vs temperature, inset: difference in density between SARW and CBMC as a function of temperature (b) Conformational transition rate normalized per torsion and time vs temperature, inset: transition rate difference between SARW and CBMC as a function of temperature (c) Radii of gyration vs temperature

We now switch our attention to studying the origin of the differences in predictions based on the amorphous builder used. Figure 3.8 compares the density, torsional transition rates and radii of gyration of polymer chains as a function of temperature for PMMA

structures containing 10 chains that were simulated with the PCFF force field; so we have ensured that the results differ only with respect to the builder used to generate the initial structure.

First, we note that the two density vs temperature curves are very similar for both simulation cases, yet when extracting T_g , values obtained for SARW structure were 20 to 50 K higher than CBMC cases, regardless of whether we use the bilinear or hyperbola approach. It is important to highlight that even though the exact same force field was used for the cooling simulations, differences in the initial structures result in small but persistence differences in torsional transition rates and radii of gyration.

Now, going back to the density results, both methods used to generate the polymeric systems started with very similar densities at high temperature (after annealing for long time), however in the case of the structure generated with SARW, the higher α_V resulted in a higher density at room temperature.

If we look at the CBMC-generated structures, they exhibited slightly higher torsional transition rates in the melt than SARW which we believe resulted in a lower glass transition temperature. The differences in radii of gyration of the systems chains are small (considerably minor than the difference resulting from the force fields) but persisted throughout the simulation, confirming the long relaxation timescales even at high temperatures. At this point, the origin in the differences observed between builders cannot be singled out.

3.4.2 Force Field

Many of the QoIs studied are related to chain dynamics and their ability to relax. For example, the glass transition is a kinetic process by which a glass is formed from a melt upon quenching and is marked by a significant increase in the relaxation timescales leading to a non-equilibrium solid. [86, 87] In polymers, this relaxation is dominated by conformational transition of torsional angles along the polymer backbone that dominate the local segmental dynamics. Thus, in order to characterize segmental mobility and relaxation, we

studied the distribution and transitions of torsion angles around sp^3 carbon atoms in the polymer backbone.

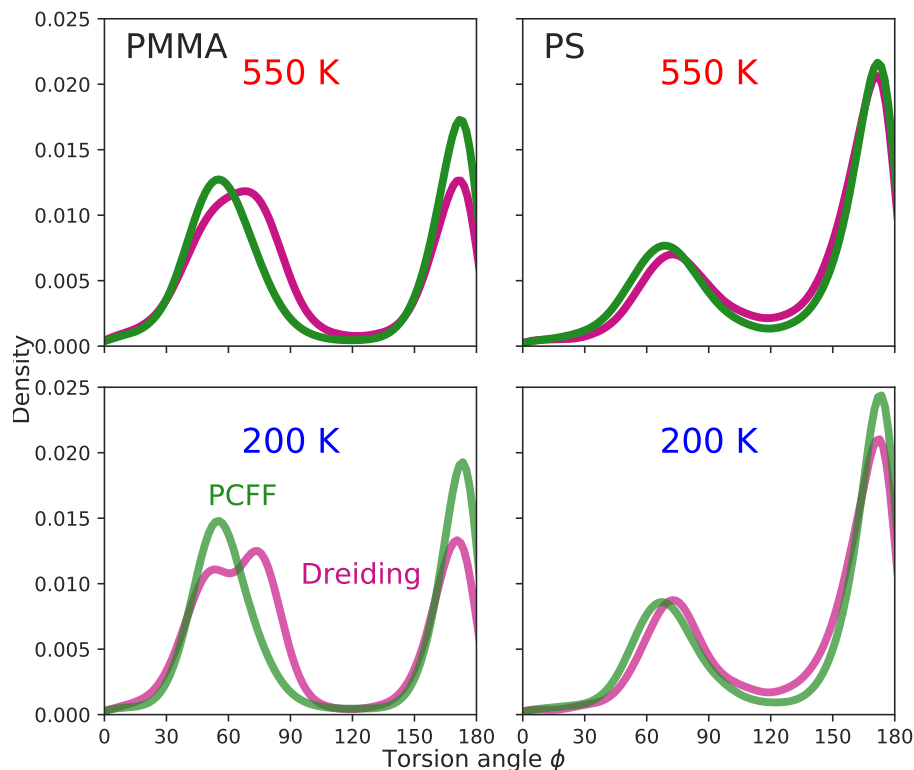


Figure 3.9.: Distribution of backbone torsional angles from MD simulations for PMMA and PS, above T_g : 550 K and below T_g : 200 K

Since the low-energy configuration around two sp^3 carbon atoms is staggered (like in ethane), the dihedral angles are expected to be 60° and 180° . Figure 3.9 shows the distribution of backbone torsional angles for PMMA and PS at two temperatures, above and below the glass transition. The figure compares results from DREIDING and PCFF for structures built using the CBMC method. In the case of PMMA we found that DREIDING resulted in broader distributions of torsional angles, indicating more flexible chains. This was not the case for PS where both force fields resulted in very similar angle distributions. Since the glass transition is related to the effective freezing of torsional degrees of freedom, [47, 88, 89] the broader distributions in PMMA for DREIDING was likely the culprit of the lower T_g

with respect to PCFF.

To confirm this, we quantified chain conformational mobility by computing the rate of torsional angles transitions between subsequent energy minimum as discussed in section 3.2.5. Figure 3.10 compares the torsional transition rates for DREIDING and PCFF in both polymers and their confidence intervals. As expected, the transition rates decrease with temperature and, in all cases, we observed a slight change in slope, around the glass transition as predicted from the density vs. temperature curves. Consistent with a broader dihedral angle distribution, in the case of PMMA the DREIDING force field exhibited a higher transition rate than PCFF above T_g .

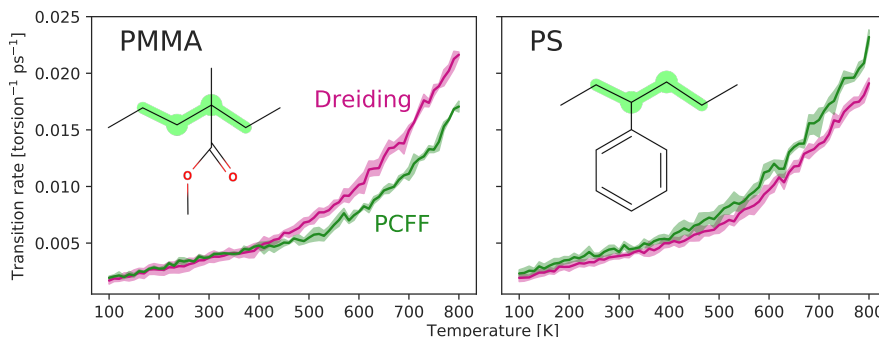


Figure 3.10.: Conformational transition rates for each force field as a function of temperature for structures built with CBMC; *left* PMMA; *right* PS

Below T_g the transition rates are comparable for both force fields. In PS, we observe slightly higher transition rates for PCFF at temperatures above 500 K. On the other hand, in PMMA we observe much higher rates at temperatures above the glass transition temperature. The latter results explain the lower T_g predicted by DREIDING for PMMA. We also analyzed the mobility of the side chains by characterizing the torsional angle distribution and transition rates. DREIDING and PCFF describe these torsions using different functional forms which results in different distributions and transition rates at high temperatures.

In order to characterize the effect of the force field on molecular structure, we quantified the radius of gyration of all chains in the various systems with 10 chains, each 70 monomers long as a function of temperature and their respective 90% confidence intervals, see Figure 3.11, and the radial distribution functions (RDFs) at 300 K, Figure 3.12. We found that DREIDING force field predicts a slightly larger radius of gyration for both polymers than the PCFF force field with a more marked difference in PMMA (approximately 20% difference vs. just over 10% for PS). The RDFs showed that both force fields led to very similar structures, the main difference being that DREIDING broadened the first peak of PS.

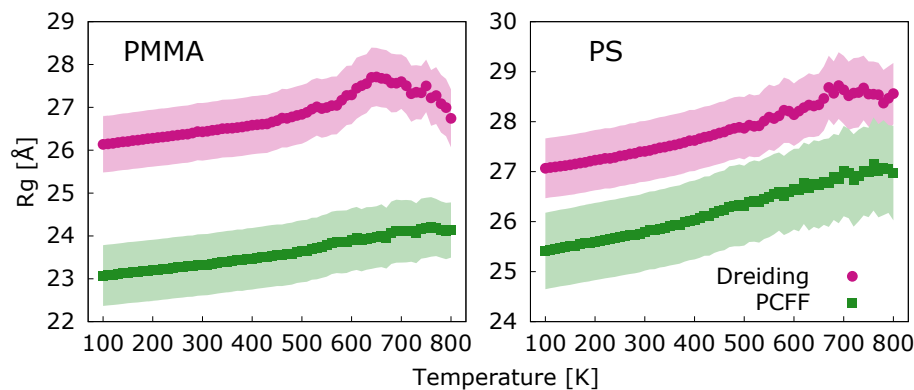


Figure 3.11.: R_g distribution averaged over the five samples built with the CBMC method and 10 chains for both polymers from MD simulations; *left* PMMA and *right* PS

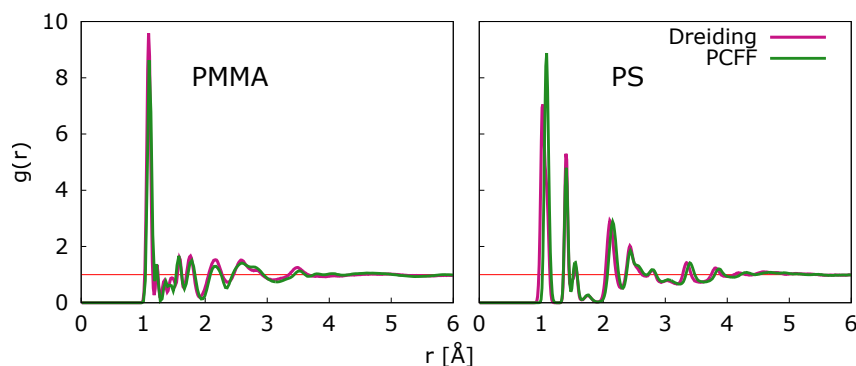


Figure 3.12.: Radial distribution functions at 300 K as a function of the force field for a sample with 10 chains; *left* PMMA and *right* PS

3.5 Glass Transition Notebook

We have created a Jupyter notebook tool as one of the deliveries in this research project. From the comprehensive study of the uncertainties in the molecular modeling of thermoplastic polymers, we have assemble the different steps required in order to predict a property. In this notebook, available at [nanoHUB](#) (listed as [Glass Transition Notebook](#)), users can build a polymer system using Polymer Modeler with pre-loaded structures or using molecular structures obtained from the materials database ChemSpider; the desire size and molecular weight can be specified. After finishing the builder step, users can perform molecular dynamics simulations using LAMMPS in order to predict T_g . All the generated systems, will include the atomic interactions as indicated in the DREIDING force field. In Figure 3.13 a collection of snapshots from the notebook is displayed; they include a visualization of the built polymer and the T_g results after MD is done.

The tool allows the users to control more advances parameters, such as the equilibration time and temperature to relax the generated structures. Additionally, the cooling rate, initial and final temperatures can be specified. The latter feature can be also helpful to understand the effect of the cooling rate on the glass transition.

As it was demonstrated previously, the data analysis plays an important role in the prediction of the glass transition. For this reason, the notebook includes a set of automatic scripts used in this work to get the raw data from the MD simulation, and extract T_g using the bilinear and hyperbola fitting methods. The error from each of the predictions is included, alongside with a plot of the density vs temperature data.

Calculate the glass transition temperature, T_g , of an amorphous polymer or molecular systems using cloud computing at nanoHUB.org

Benjamin Haley, Lorena Alzate-Vargas, Martin Hunt, Chunyu Li, and Alejandro Strachan
Purdue University

Three four main steps to calculate T_g :

1. Build an atomistic model for your molecular material using Polymer Modeler (nanohub.org/tools/polymod)
2. Relax the structure using molecular dynamics (with LAMMPS) at a relatively high temperature (above the expected T_g)
3. Use molecular dynamics to cool down your system (we will identify T_g as a change in slope in the density-temperature data)
4. Fit the density-temperature data using a bilinear and hyperbola functions and extract T_g

Further reading

- Uncertainties on predictions of thermo-physical properties of thermoplastic polymers via molecular dynamics, Alzate-Vargas, Lorena; Fortunato, Michael; Haley, Benjamin; Li, Chunyu; Colina, Coray; Strachan, Alejandro, Mod. Sim. Mat. Sci. Eng. (2018).
- Atomistic simulations of amorphous polymers in the cloud with PolymerModeler, Haley BP, Li C, Wilson N, Jaramillo E, Strachan A. arXiv preprint arXiv:1503.03894. 2015 Mar 12.

```
# System setup
import sys, os, tempfile, numpy as np
import hubble.rappture as rappture
sys.path.append('/apps/share64/debian7/ipyntools')
import hubwf
```

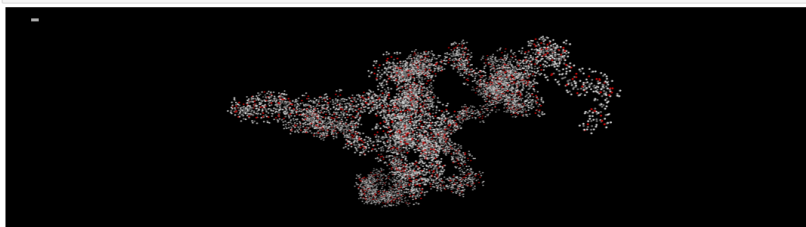
Step 1. Build an atomistic model of your polymer or molecular system

```
# Create an interface to the PolymerModeler tool
task = rappture.Tool('polymod')

# This variable selects the source of the monomer molecule(s). By default, we use monomers already defined in the PolymerModeler
# on nanohub, but we can also download molecular structure files from ChemSpider.
monomer_source = 'polymod'
#monomer_source = 'chemspider'
```

Polymer system after building

```
# View the initial structure built by PolymerModeler
task.get_output('Built structures, unwrapped').plot()
```



Get results

Tg from bilinear fit: 363 Error: 5.8
Tg from hyperbola fit: 352 Error: 9.57

Figure 1

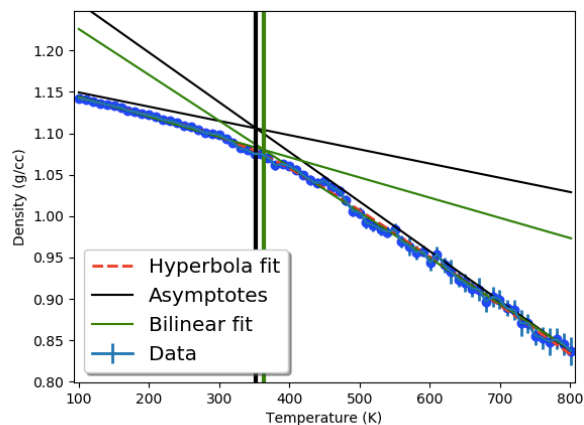


Figure 3.13.: Snapshots of the Glass Transition Notebook as displayed at [nanohub](http://nanohub.org) including the visualization of built polymer system and results

3.6 Conclusions

As in any physics-based simulations, uncertainties in predicted materials properties obtained from molecular-level simulations of molecular materials are inevitable. These uncertainties originate from various sources, including molecular force field form and parameters used to describe atomic interactions, sampling size, molecular structure (in the case of amorphous polymers this includes chain molecular weight and the method used to build the initial structure), and numerical analysis method. These uncertainties also depend on the specific chemistry of the molecular system investigated and the property of interest. We found that the force field used to describe atomic interactions is the main variable affecting density while the extracted glass transition temperature is affected quite significantly by the amorphous builder, data analysis method, and chain molecular weight. Also, sample to sample variability is quite significant even for the relatively large samples studied. We found a correlation between predicted T_g and density between the two force fields studied (PCFF and DREIDING): higher density results in higher T_g . Interestingly, the method to extract from the simulations also results in significant uncertainties; large differences in the extracted quantity from different methods can indicate issues in the underlying data.

4. MOLECULAR MODELING OF SMALL ORGANIC CRYSTALS

ADAPTED FROM:

Yifei Zeng et al. 2019 Modelling and Simulation in Materials Science and Engineering, **27**, 074005 © 2019 IOP Publishing Ltd.

4.1 Introduction

Milling and micronization are commonly used to reduce the particle size of active pharmaceutical ingredients. [90] During these processes the materials are subjected to extensive deformation that may result in amorphization. [91–93] Current amorphization models require multiple parameters, demanding a large number of experiments. In spite of that, the use of multiscale frameworks, that integrate numerical tools across different length scales can help to reduce the necessity of experimental data.

A proposed multiscale methodology to predict mechanically induced amorphization without experimental information, including molecular dynamics simulations, dislocation dynamics (DD) simulations and phase fields models (PF) is described in this chapter.

From the MD simulations, the melting temperature, enthalpy of fusion, crystal-amorphous interface energy, and elastic constants are calculated for small organic crystals. Subsequently, this information is used in a phase field model that includes defect nucleation and solid state amorphization to predict whether the crystal will amorphize or not.

Here we discuss the prediction and validation of some properties of known small organic crystals in order to verify the simulations performed. This was extended to predict the response of two pharmaceutical compounds F1 and F2 (Fig. 4.1), without any experimental information.

This Work was done in collaboration with Chunyu Li and it was published in Modelling and Simulation in Materials Science and Engineering as coauthor with Yifei Zeng, Rachel Graves, Jeff Brum, Alejandro Strachan and Marisol Koslowski coauthors [94]

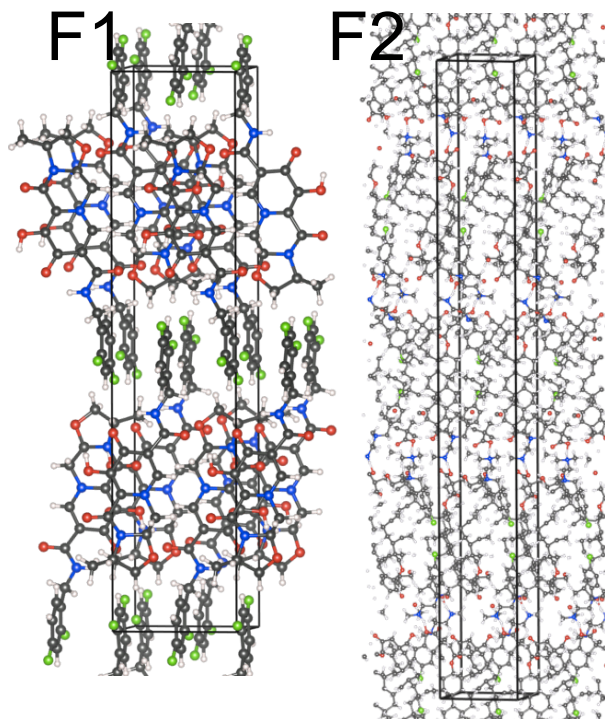


Figure 4.1.: Crystalline structure of compounds F1 and F2

4.2 Simulation Details

Molecular dynamics simulations were performed using LAMMPS. [71] The crystal structures were obtained from the Cambridge Structural Database and we used an in-house set of scripts comprised in the [LAMMPS data file generator](#) [61] tool, in order to determine covalent bonds, identify atom types and assign the appropriate force field parameters, see [2.2.1](#) for more details.

DREIDING force field [56] was used to describe atomic interactions with environment dependent partial atomic charges obtained using the QEq method [95] with parameters from Reference [96]. The non-bonded van der Waals interactions are described using the Buckingham potential with an exponential repulsion and power sixth attraction with a cutoff of 12 Å and explicit hydrogen bond interactions described using LJ potential form 12/10 with a cutoff of 6.5 Å. The non-bonded long-range electrostatic interactions were described

using the particle-particle, particle-mesh method with a precision of 10^{-4} kcal/mol.Å. A time step of 1 fs was used in all the simulations.

The initial structures were replicated to obtain simulation boxes of the desired size, based on a considerable number of atoms. Later, they were relaxed via energy minimization; followed by a two step thermal equilibration at 300 K, first on a NVT simulation for 50 ps and last NPT run for 200 ps.

In order to obtain the properties of the amorphous phase of the materials of interest, we used the melt and quench method. The equilibrated crystal structures were heated up to 1000 K under NPT conditions, well above the expected melting temperatures, with a heating rate of 10 K/200 ps. Succeeded by a 100 ps of NVT relaxation to enhance the equilibration of the liquid sample and to confirm their molten state. Cooling procedure is done using NPT conditions at a rate of 10 K/50 ps.

4.3 Predicted Properties in Organic Crystals

Table 4.1 contains the lattice parameters from MD simulations compared to experimental results for various small organic crystals. Figure 4.2 shows snapshots of γ -indomethacin in the crystal and amorphous form and the density vs temperature during the heating/cooling cycle. We estimated the glass transition temperature T_g , from the change in slope in the curve during cooling. Our predicted value is approximately 360 K, just above the experimental result 323 K. [97]

From the MD simulations we obtain the energy and volume during the isobaric heating and cooling process to calculate the enthalpy of fusion between a crystalline bulk and its amorphous counterpart calculated as

$$\Delta H = \Delta U + P\Delta V \quad (4.1)$$

Table 4.1.
Predicted MD lattice parameters and experimental values for various small organic crystals

| Compound | Unit cells | Molecules | Predicted | | | | | | Experimental | | | | | |
|-------------------------------------|---------------|-----------|----------------|----------------|----------------|---------------------|--------------------|---------------------|----------------|----------------|----------------|---------------------|--------------------|---------------------|
| | | | $a/\text{\AA}$ | $b/\text{\AA}$ | $c/\text{\AA}$ | α/deg | β/deg | γ/deg | $a/\text{\AA}$ | $b/\text{\AA}$ | $c/\text{\AA}$ | α/deg | β/deg | γ/deg |
| Acetaminophen ¹ | 27 | 216 | 16.798 | 12.705 | 7.707 | 90.0 | 90.0 | 90.0 | 17.156 | 11.831 | 7.405 | 90.0 | 90.0 | 90.0 |
| γ -indomethacin ² | 27 | 54 | 9.328 | 11.008 | 9.777 | 69.4 | 110.8 | 92.8 | 9.295 | 10.969 | 9.742 | 69.4 | 110.8 | 92.8 |
| Aspirin ³ | 45 | 180 | 11.548 | 6.659 | 11.513 | 90.0 | 95.7 | 90.0 | 11.446 | 6.596 | 11.388 | 90.0 | 95.3 | 90.0 |
| Salicylamide ⁴ | 50 | 200 | 6.177 | 4.381 | 25.289 | 90.0 | 90.0 | 90.0 | 5.561 | 3.893 | 28.566 | 90.0 | 90.0 | 90.0 |
| Sucrose ⁵ | 32 | 64 | 8.133 | 9.140 | 11.399 | 90.0 | 102.9 | 90.0 | 7.762 | 8.704 | 10.863 | 90.0 | 102.9 | 90.0 |
| Compound F1 | 50 | 200 | 7.400 | 7.813 | 32.378 | 90.0 | 90.0 | 90.0 | 7.2597 | 7.2928 | 32.276 | 90.0 | 90.0 | 90.0 |
| Compound F2 | 16 | 128 | 11.028 | 11.064 | 80.767 | 90.0 | 90.0 | 90.0 | 10.658 | 10.658 | 84.906 | 90.0 | 90.0 | 90.0 |

¹ Ref. [98]

² Ref. [99]

³ Ref. [100]

⁴ Ref. [101]

⁵ Ref. [102]

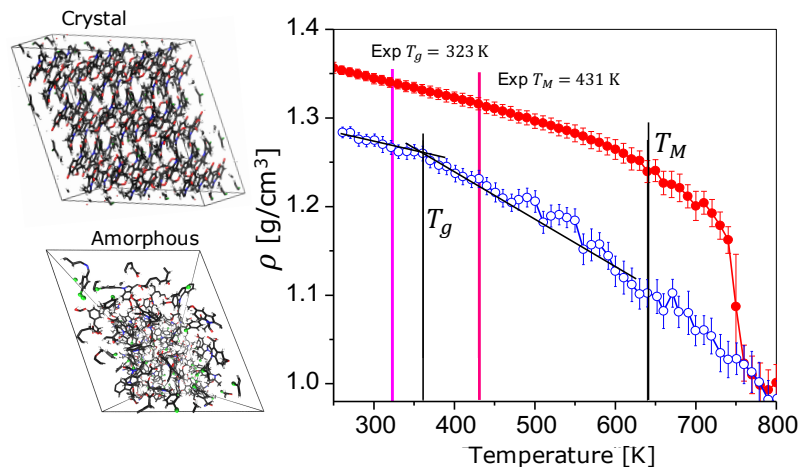


Figure 4.2.: γ -indomethacin crystal and amorphous structures and density changes during heating and cooling with predicted glass transition and melting temperature

where H stands for enthalpy, and U , P , V for potential energy, pressure and volume, respectively.

Melting Temperature The solid-liquid coexistence method [103] was adopted to predict the melting temperature T_M . The preparation of a crystal-amorphous coexistence simulation system consists in beginning with a relatively large pure crystal system, then removing a third of the molecules at one extreme and center to create interfaces and empty space. A third of the crystal molecules is kept fixed and the remaining third is heated to get a liquid region. Finally, the solid/liquid coexistence is quenched to 400 K and relaxed for 2 ns under anisotropic NPT conditions. A solid/liquid configuration and the volume vs temperature data for γ -indomethacin is shown in Fig. 4.3.

To predict T_M , the relaxed crystal-amorphous structure is taken to a series of temperatures under NPT condition for 400 ps. At temperatures above the melting point the liquid phase will grow at the expense of the solid increasing the volume of the sample and the opposite will occur at temperatures below T_M . The normalized volume by $V(T = 300 \text{ K})$ vs temperature is used to extract T_M as the intersection of two segments.

Amorphization enthalpy In order to assess the propensity of the various compounds to *amorphize*, Figure 4.4 shows the amorphization energy predicted by the MD simulations at T_M . The high enthalpy of amorphization of salicylamide, acetaminophen and aspirin indicates little propensity to amorphization whereas sucrose and γ -indomethacin are more likely to exhibit amorphization, this is consistent with experimental studies. Compound F1 has a lower amorphization enthalpy than aspirin and slightly higher than sucrose, whereas the predicted value for F2 shows more tendency towards amorphization.

To validate the results of our MD simulations performed in acetaminophen, aspirin, salicylamide, γ -indomethacin, and sucrose; we compared our results with available experimental data for each compound, see Figure 4.5. The experimental density values for F1 and F2 were obtained by x-ray diffraction of single crystals. Overall our predicted values are in good agreement with the experimental data reported in literature. The crystal density obtained from our simulations shows an excellent agreement for γ -indomethacin, sucrose, salicylamide and aspirin with the experimental data. We notice that our predicted T_M corresponds with the experimental data, which validates the method implemented, being Aspirin an exception due to its large deviation, it was later found that the charge equilibra-

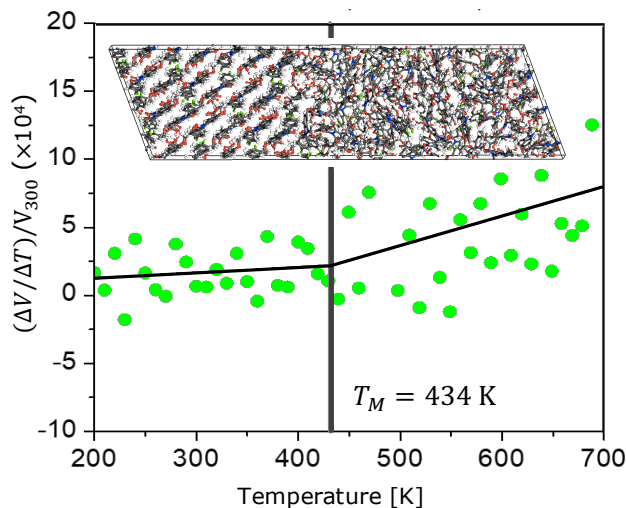


Figure 4.3.: Coexistence of crystal and amorphous structures and the determination of melting temperature in γ -indomethacin

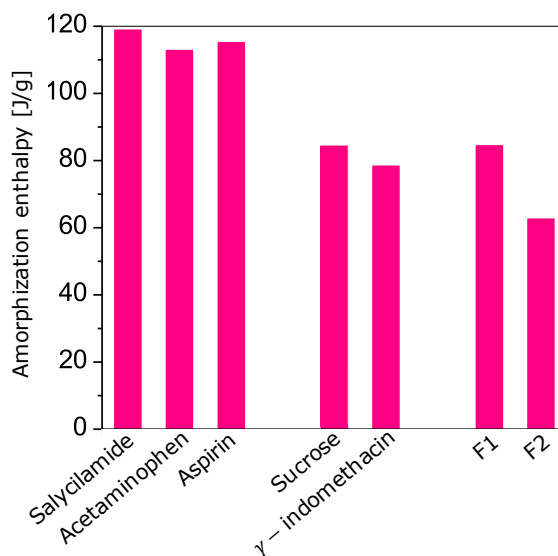


Figure 4.4.: Calculated amorphization enthalpy from MD simulations

tion parameters used might have impacted the simulations performed for calculating the melting temperature. The predicted melting temperatures for compounds F1 and F2 are 480 K and 450 K, respectively, it is important to mention that no experimental values for this quantity are available similarly for the enthalpy of fusion ΔH_f . we observe that the predicted ΔH_f are very close to the experimental data, mostly due to the super-heating at the melting temperature.

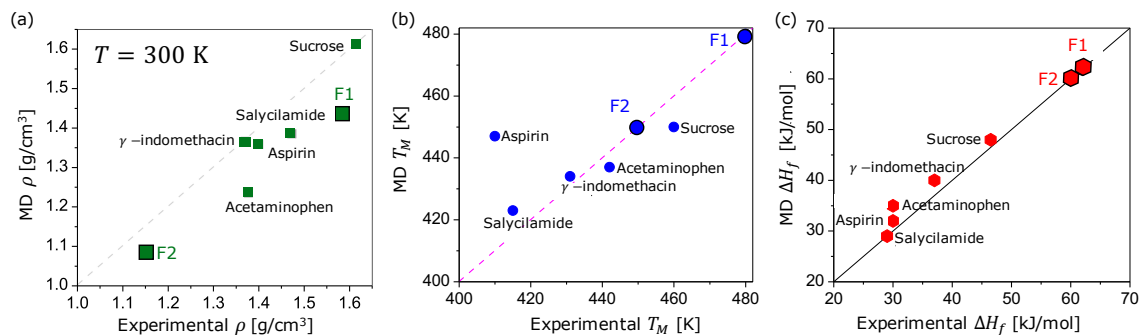


Figure 4.5.: Validation of predicted properties using MD for various small organic crystals (a) density at room temperature, (b) melting temperature, and (c) enthalpy of fusion

4.4 Conclusions

With the provided information from MD simulations that were validated in multiple compounds; dislocation dynamics (DD) and finite element analysis (FEA) models were used to predict amorphization of molecular crystals, achieving successful results, particularly in compounds F1 and F2. It was found that compound F1 does not exhibit any noticeable increase in the volume of the amorphous regions while F2 shows an increase of the amorphous phase. Physical tests were performed for each compound. Most notably gravimetric vapor sorption showed that F2 exhibited behavior consistent with amorphization.

5. LOCAL CHAIN DYNAMICS AND GLASS TRANSITION IN POLYMERIC BULK AND FINITE SIZE SYSTEMS BY MOLECULAR DYNAMICS SIMULATIONS

5.1 Introduction

Due to the experimental evidence that proves the existence of spatially heterogeneous dynamics (see discussion in section 1.1), and despite significant progress in understanding the glass transition phenomenon, the molecular level processes responsible for the slowdown of the relaxation dynamics, so called α -relaxation in polymers is not well understood. For this reason, computer simulations have been used to provide some insight into the nature of dynamic heterogeneities.

Several simulation works have reported evidence of organized motion in supercooled liquids [43, 45, 104, 105] and granular systems, [104, 106] where particles that undergo large displacements (hopping) on fast time scales tend to arrange in clusters [42] as an indicator of the cooperative motion responsible for the relaxation of a liquid above its glass transition. Molecular dynamics simulations can provide a microscopic level understanding of the local relaxation phenomena in polymers not available experimentally. Several studies have monitored the evolution of torsional angles and their conformational transitions in bulk polyethylene, [46–48, 50, 107] polypropylene, [49, 88] and poly(methyl-methacrylate) [108] correlating this motion with the dynamic relaxation.

These MD simulations confirmed the existence of cooperative motion at temperatures near T_g , Arrhenius behavior of conformational transitions, a noticeable freezing of dihedral angles below T_g with an increase in heterogeneity of conformational dynamics. [46, 49, 50, 52] Recent MD simulations have proved a linear relationship between activation energy E_a of torsional transitions and glass transition temperatures for bulk polymers. The E_a values obtained correspond to the energy required for a dihedral angle to go from the *gauche* state

to the *trans* state. Higher activation energies have been connected to cooperative effects in torsions. [51] We observe this behaviour in our work as well. However, the cooperative behavior of torsions where transitions are found in clusters, with characteristic length and time scales in polymers has not been addressed. In the addition little is known regarding how the characteristics of theses process translate to nanoscale specimens.

In this work we investigate spatial and temporal correlations in the mobility of backbone torsional angles from MD simulations of various bulk and finite-sized polymers. A cluster analysis of the transitions in torsional angles along the polymers backbones reveals a percolation critical phenomena from plentiful isolated high-mobility domains below T_g to a large percolating cluster. Quite interestingly, we find nearly identical transitions in the bulk polymers studied, in nano-scale slabs and in free-standing chains. This indicates that key characteristics of the glass transition survive down to isolated and relatively small chains.

5.2 Computational Details

5.2.1 Polymeric Systems

We characterize the dynamical relaxation of atactic poly(methyl-methacrylate) (PMMA), atactic polystyrene (PS), atactic polypropylene (PP) and polyethylene (PE) bulk samples. In the case of PMMA we study the effect of chain molecular weight and finite size effects in slabs and single-chain systems. For bulk polymers mentioned previously, we studied samples with 40 chains and 100 monomers per chain. Additionally, PMMA samples were also investigated. They are listed below.

- (i) a bulk systems with 4 chains with 1000 monomers per chain,
- (ii) a slab system of 40 chains and 60 repeating units each, and
- (iii) two isolated chains: 100 monomers and 1000 monomers.

All samples were built using the continuous configurational bias Monte Carlo (CBMC) as implemented in the Polymer Modeler tool available for online simulations at [nanoHUB](#).

5.2.2 Molecular Dynamics Simulations

The bulk structures were generated at an initial density of 0.5 g/cm^3 . The PMMA slab sample was built with periodic boundary conditions in x and y directions and two excluded regions along the z-direction; polymer chains are reassigned in the box to reach an initial density of 0.4 g/cm^3 . To generate isolated polymeric chains, a single chain was built and placed in the center of a large box (to avoid mirror images) but keeping periodic boundary conditions along the three directions.

To relax each resulting configuration, a 3-level step energy minimization with scaled van der Waals parameters was performed, followed by a thermal equilibration at 600 K. The latter procedure consists of a simulation under NVT conditions for 50 ps and a second run with NPT ensemble (pressure of 1 atm) for 500 ps. We monitored that the density reaches equilibrium. However, we must clarify that the procedure for isolated chains was different and involved one single NVT simulation for 500 ps.

After thermalization, each structure was cooled keeping the equilibration ensemble in a step wise manner. Temperature was decreased every 10 K, and held during 100 ps, until reaching a final temperature much below the expected glass transition temperature. For PMMA and PS the final temperature is 200 K; for PP final temperature is 100 K and for PE is 50 K. The final atomic structure at each temperature was taken for an extended run during 1 ns; an atomic snapshot was recorded every 2 ps for further analysis.

All MD simulations are carried out using LAMMPS. [71] Atomic interactions were calculated using the DREIDING force field [56] and atomic charges were obtained using the Gasteiger partial charge algorithm. [69] Non-bonded long-range electrostatic interactions were described using the particle-particle, particle-mesh method with a precision of $10^{-4} \text{ kcal/mol.Å}$ and the non-bonded van der Waals interactions are described using the Buckingham potential with an exponential repulsion and power sixth attraction with cutoff of

12 Å. A time step of 4 fs was used in all the simulations.

Our goal is to detect transitions in dihedral angles along the polymers backbone and assessing spatial and temporal correlations between them. This is accomplished in two steps using developed Python in-house codes, first we identify torsional transitions from the atomistic trajectories and second, we perform a cluster analysis in space and time.

5.2.3 Torsional Transition Analysis

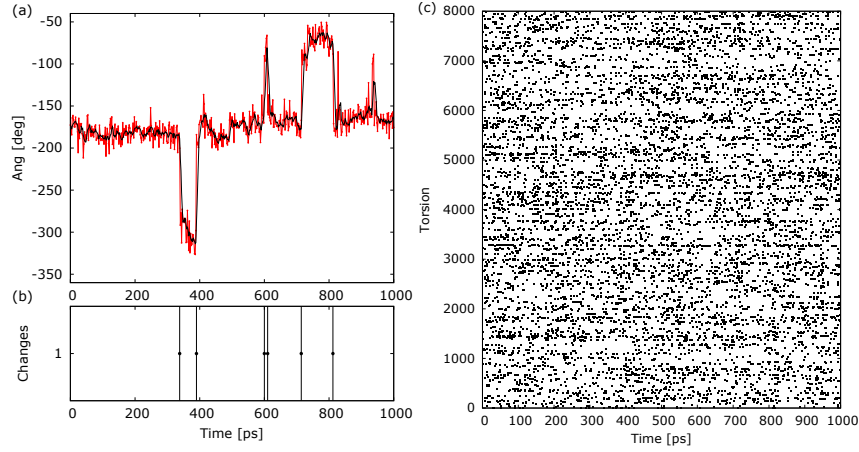


Figure 5.1.: Torsional transition analysis. (a) Time evolution of a backbone dihedral angle obtained from the MD trajectory every 0.1 ps (red line). A window average has been performed to obtain a torsional angle every 2 ps shown as black line. (b) Jumps detected for the monitored angle. (c) All transitions (black points) found for backbone dihedral angles as a function of time in bulk PMMA at 480K

We calculated the time evolution of the torsional angles for each dihedral along the backbone chain, from the positions of four consecutive sp^3 carbon atoms, from the MD trajectory recorded following the same methodology proposed in 3.2.5. We monitored the time evolution of each torsional angle with a time resolution of 2 ps simplifying the detection of a jump. A transition has occurred at time t if :

$$\Delta\phi [(t_i + 2 \text{ ps}) - (t_i - 2 \text{ ps})] \geq 80^\circ$$

Figure 5.1 shows the time-evolution trajectory of a dihedral and their respective conformational jumps. All the active transitions that were identified during a 1 ns simulation of bulk PMMA at $T = 480$ K are shown in (c).

5.2.4 Cluster Analysis

In order to characterize spatial-temporal high-mobility domains we performed a cluster analysis on active torsions in space and in time, via an in-house code implementing minimum spanning tree algorithm. Every time torsion undergoes a transition we define an active torsion, i , and characterize it by a position in the simulation cell (R_i , the center point between the two central atoms) and a time (t_i). Two active torsions, i and j , are defined to belong to the same cluster if:

$$|R_i - R_j| \leq R_c \text{ and } t_i = t_j$$

or

$$I_i = I_j \text{ and } |t_i - t_j| \leq t_c$$

Where I_i represents the index of = active torsion i , R_c is a cutoff in space and t_c is the temporal cutoff. The cluster analysis was performed with temporal cutoff $t_c = 8, 16, 32$ and 64 ps for a various distance cutoffs.

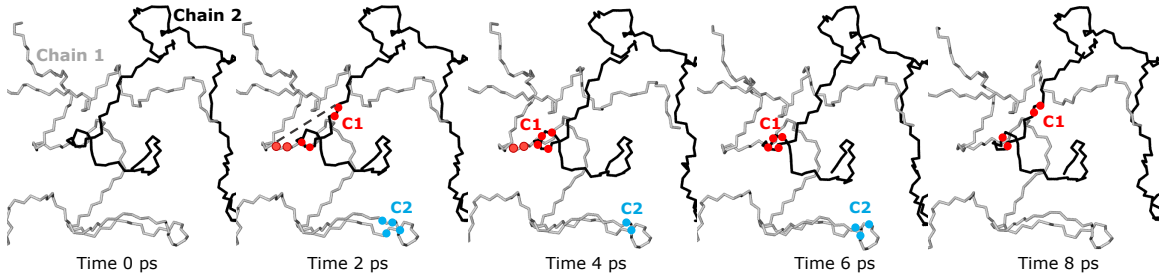


Figure 5.2.: Cluster analysis procedure visualization. Two clusters of active torsions (C1 and C2) are detected within space cutoff at $t = 2$ ps, at consecutive times (until reaching cutoff) we monitored the same torsions and nearby ones so they will be included in initial identified clusters

Figure 5.2 shows the time evolution of two high-mobility clusters represented by circles, formed by nearby torsions that belong to two different chains in a time window of

8 ps.

At $t = 0$ no active torsions are found. Two clusters of active torsions in space are detected at $t = 2$ ps. Subsequently, at time $t = 4$ ps, some torsions undergo transitions and remain active, so they are added to the initial cluster; this is repeated with the torsions that transitioned at $t = 6$ ps and $t = 8$ ps.

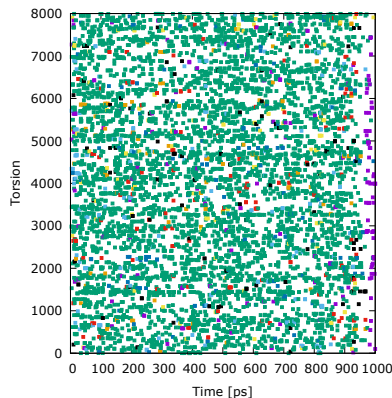


Figure 5.3.: Active backbone torsions as a function of time in PMMA at 480K after clustering analysis. Each color represents a cluster identified in the simulation, however torsion index does not represent the location in space of the dihedral angles

For visualization purposes, Figure 5.3 shows the transitions detected in Fig. 5.1b after the cluster analysis is performed. Each color represents a spatio-temporal cluster detected, however torsion index does not reflect the actual location of the angle in the simulation. As the temperature is above the glass transition we can see one predominant cluster (green) with most of the active torsions.

5.3 Torsional Relaxation in Bulk Systems

In order to characterize the bulk systems studied, we calculated the glass transition temperature from the density vs. temperature data obtained by averaging the last 50 ps of the MD simulation at each temperature during the cooling procedure.

We have used the bilinear and hyperbola fitting methods described in 3.2.4 to compute T_g ; results are summarized in Table 5.1 and they are also displayed in Fig. 5.4. Our predictions

are in good agreement with the experimental data after the effects of cooling rate in MD are taken into account.

Table 5.1.
Predicted glass transition temperatures T_g [K] from MD simulations for bulk samples using two fitting procedures

| | PE | PP | PS | PMMA |
|---------------|-----|-----|-----|------|
| Bilinear fit | 195 | 246 | 442 | 453 |
| Hyperbola fit | 208 | 275 | 456 | 479 |

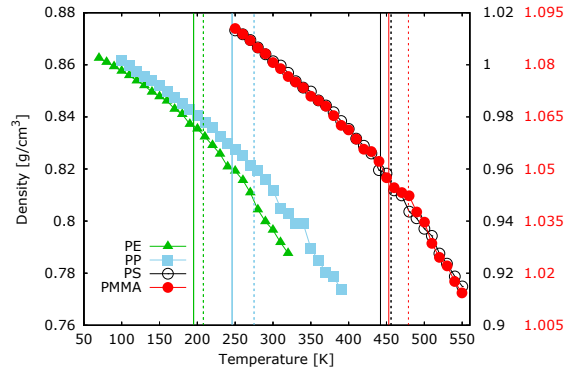


Figure 5.4.: Density vs. temperature data for each polymer and computed glass transition temperature. Solid lines and dashed lines represent results from the bilinear and hyperbola fitting procedure respectively

We obtain torsional transition rates k at each temperature as the number of active torsions normalized by the total number of backbone torsions in each system and total simulation time following Equation 3.2. Figure 5.5a compares the transition rate for bulk systems of PMMA, PS, PP and PE consisting of 40 chains with 100 monomers; with their respective glass transition regimes. Notice, that the rate of conformational transitions is very similar in both PMMA and PS; this is consistent with the fact that they have similar glass transition temperatures. While all systems exhibit similar trends of reduction of torsional transition rates with decreasing temperature, the rates at T_g are different for each

polymer. In Fig. 5.5b we plotted the same results using an Arrhenius form for each bulk polymer studied.

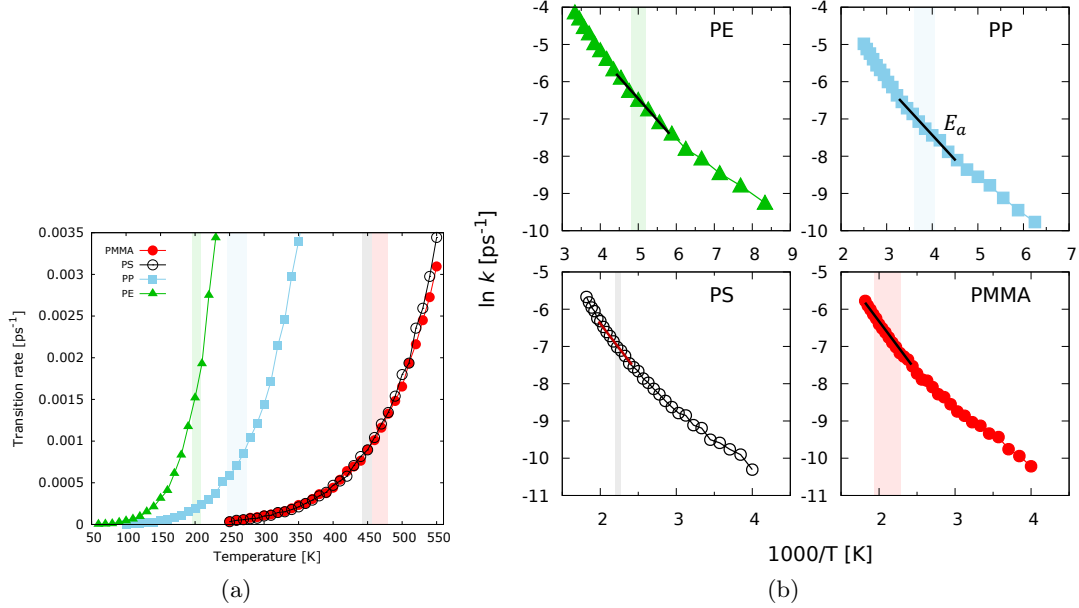


Figure 5.5.: Conformational transition rates as a function of temperature for bulk polymeric samples. (a) Torsional transition rates vs. temperature; shadow regions represent glass transition regimes and, (b) Transition rates as a function of temperature in Arrhenius form for each polymer

To calculate the activation energy associated with the motion of the backbone chain and relate with the glass transition temperature, we calculated the slope from $k(T) \propto \exp(-E_a/RT)$ in Fig. 5.5b following the form in Equation 5.1. A linear regression was done in the region between T_g^{bilinear} and $T_g^{\text{hyperbola}}$.

The correlation between E_a and T_g for bulk polymers in this work is shown in Figure 5.6 is consistent with the demonstrated linear relationship proposed in Ref [51], on the form of $E_a[\text{kcal/mol}] = 0.01T_g + 0.44$ according to results in bulk PE, PS and PVDF. Despite that it has been suspected that the activation energies correlate with a single barrier value

(the energy required for a torsion bond to go from one configurational state to another) it will be later shown that cooperative effects play an important role.

$$\ln k = -\frac{E_a}{R} \frac{1}{T} + \ln A \quad (5.1)$$

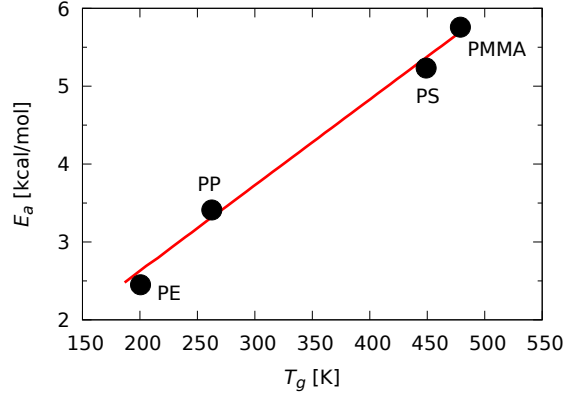


Figure 5.6.: Activation energy (E_a) from backbone torsions as a function of bulk T_g

Having established overall trends of average torsional mobility and their relationship with T_g , we now study the spatio-temporal correlations between active transitions by means of the cluster analysis described in 5.2.3. For visualization purposes, snapshots of the active torsions in bulk polystyrene at 460 K at different times are shown in Fig. 5.7.

We previously discussed the use of several temporal cutoffs to aggregate the active torsions and to assess the characteristic scales of the problem.

In order to select appropriated distance cutoffs for the various polymers we computed the radial distribution functions (pair correlation functions) between torsion centers for each system, see Figure 5.8 including results for PMMA and PS at 450 K and for PP and PE at 260 K and 200 K respectively. The sharp peaks at short distances correspond to nearby torsions along the polymer backbone, the broader peaks correspond to non-bond distances. Following this analysis, we selected a cutoff to include the first two non-bond peaks; as expected, observation of percolation requires cutoffs long enough to capture torsions in

nearby chains.

The resulting cutoffs are: 20 Å for PMMA, 22 Å PS, 15 Å in PP, and 11 Å for PE. Our characteristic lengths are in agreement with experiments and models for bulk polymers.

Using these spatial cutoff we have performed the cluster analysis with a temporal cutoff of 64 ps. The torsional transition rates are calculated based on two types of motion:

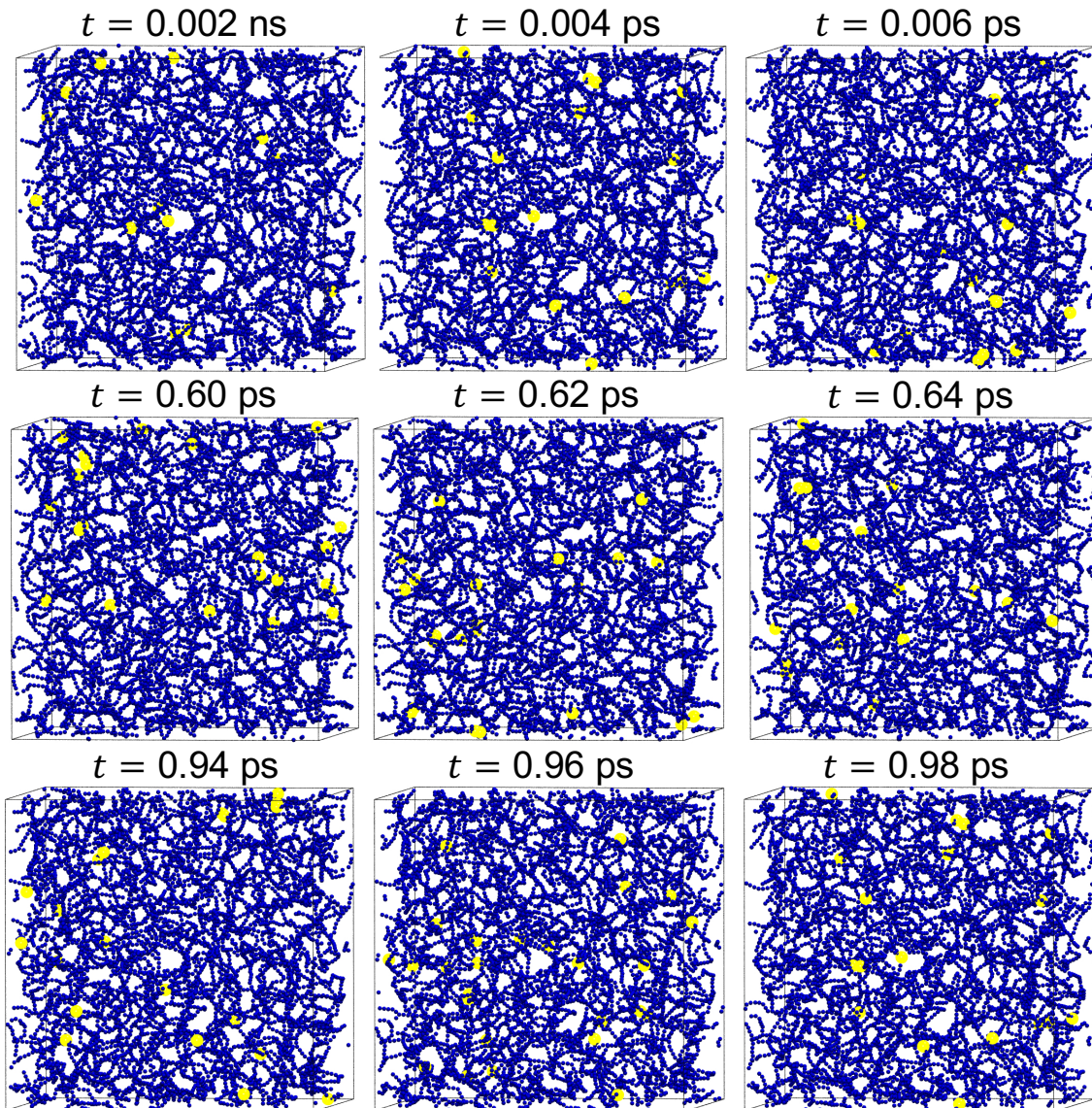


Figure 5.7.: Snapshots of bulk polystyrene at 460 K with active torsions in yellow. The blue points represent the torsion centers along the backbone chain

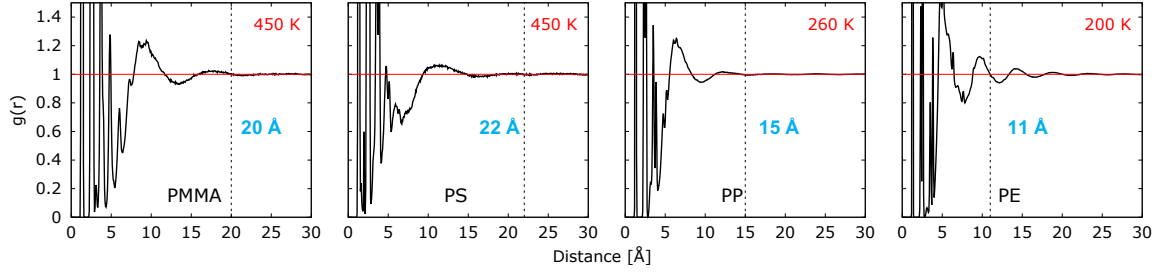


Figure 5.8.: Radial distribution function of backbone torsions in bulk PMMA at 450 K, PS at 450 K, PP at 260 K, and PE at 200 K

(1) Isolated transitions, identified as single torsion clusters, and, (2) Cooperative transitions, corresponding to several torsions correlated in space and time. In Figure 5.9 we exhibit the transition rates vs temperature for bulk polymers according to the clusters they belong to. At low temperatures, the rate is mainly governed by single clusters, whereas at high temperatures, the overall transition rates are dominated by cooperative torsions. We have split the cooperative jumps into ones that are associated in clusters with number of torsions between 2 and 10 and clusters with more than 10 active torsions. At temperatures around the glass transition regime an increase in small size clusters is more prominent. As expected, the low temperatures are governed by isolated transitions whereas the high temperatures are mainly dominated by the cooperative behavior of torsions.

The intersection of isolated and cooperative transition rates is consistent with the predicted T_g .

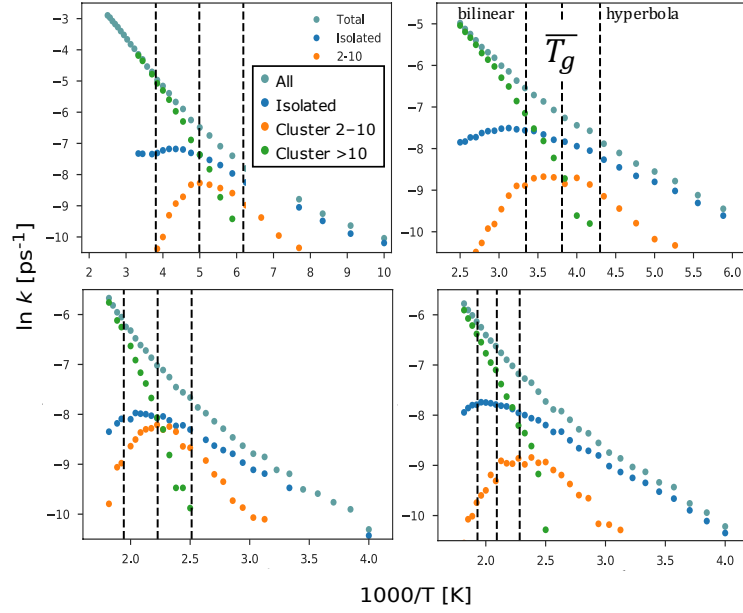


Figure 5.9.: Torsional transition rates $\ln k$ with respect to cluster size vs. temperature $1000/T$ for bulk polymers using $t_c = 64$ ps. The predicted T_g s from bilinear and hyperbola fits and the averaged value are shown as dashed lines

Figure 5.10 shows the time-averaged cluster size (defined as the number of active torsions per time) for each cluster as a function of temperature (colored points) and the mass-weighted average size over all clusters, black symbols. As expected, the average cluster size increases with temperature, but, quite interestingly, the size of the largest cluster of active torsions grows considerably faster than the rest starting a temperature around the glass transition, described as gray color regions in Fig. 5.10. This behavior is typical of percolation. In the same manner, the weighted-average lifetime of clusters calculated as $t(\text{final torsion}) - t(\text{initial torsion})$ is displayed in Figure 5.11. Consistent with the increase of number of torsions in the cluster, around T_g the duration spans almost all the simulation time.

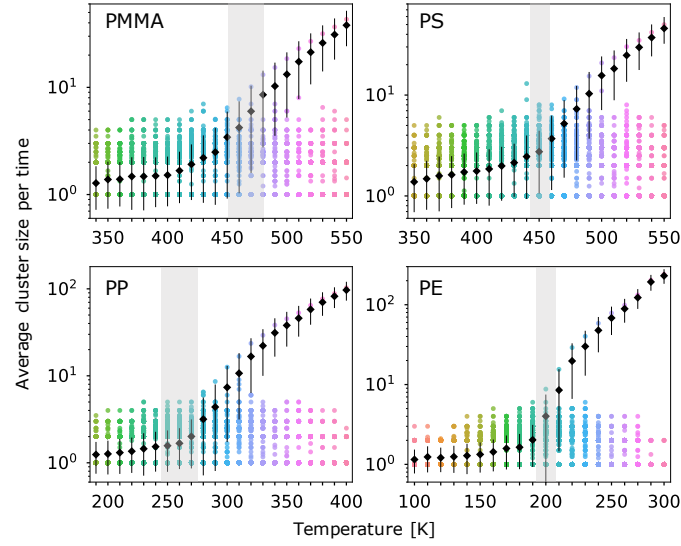


Figure 5.10.: Average cluster size defined as number of torsions normalized per time over all clusters in log-scale (black points) corresponding to $t_c = 64$ ps and defined R_c for bulk samples. Colored points show the distribution of cluster sizes per time as a function of temperature. Size of a mobile cluster grows as $T \rightarrow T_g$ in concordance with the percolation behavior

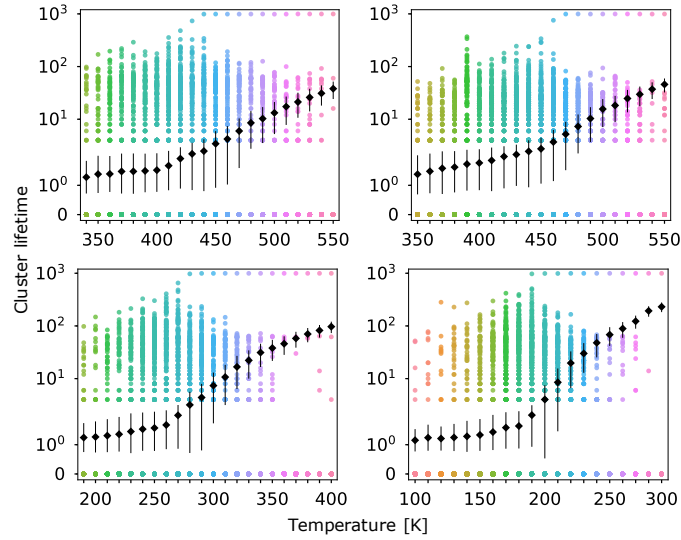


Figure 5.11.: Average cluster lifetime (last time active torsion - first time active torsion) in black points. The distribution of cluster duration is shown in colors

To characterize the percolation of the active domains, we define the strength of the largest cluster, defined as its size as a fraction of the total number of active torsions, as a function of temperature. Figure 5.12 shows the strength as a function of temperature in bulk polymers for several temporal cutoffs. Interestingly, we observe nearly identical percolation behavior in all systems. At low temperatures, relaxation dynamics are governed by large numbers of relatively small high-mobility domains; thus, the strength of the largest cluster is near zero. As temperature is increased and clusters of active torsions merge, a percolating high-mobility domain forms and the size of this large domain increases above a critical temperature. As in all percolation problems, the critical temperature depends on the cutoff used to define clusters [109]. Despite this dependence, the percolation of a mobile domain occurs approximately around the glass transition temperature. In order to verify the characteristic scales of the problem, we have performed the cluster analysis with different spatial and temporal cutoffs as displayed in Fig. 5.13.

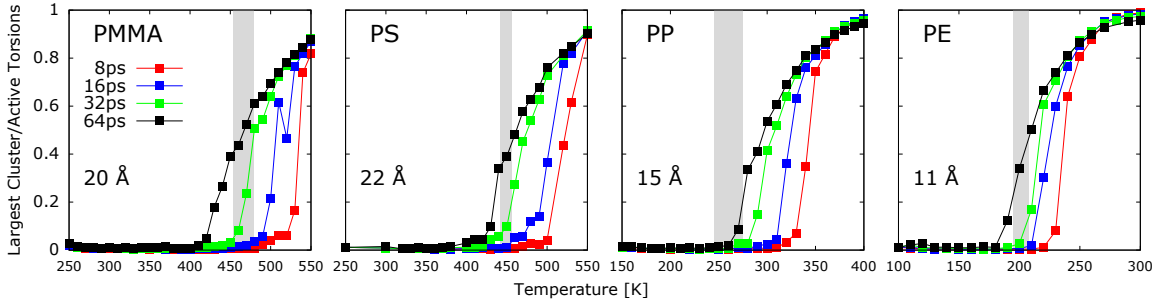


Figure 5.12.: Largest cluster normalized by active torsions as a function of temperature at different t_c using selected distance cutoff

We find it instructive to visualize correlations between active torsions as shown in Figure 5.14. We show all active torsions as a function of time, the torsion index (vertical axes) is unique and assigned sequentially as torsions become active, importantly colors represent clusters. We find significant correlations between active torsions in the glassy state, denoted by groups of dots with the same color. Increasing temperature results in a larger number of active torsions but also in the formation of larger, correlated clusters, indicating domains of high mobility. At high temperatures, right above the glass transition,

a large cluster is formed accompanied by small clusters which eventually will become part of the same cluster.

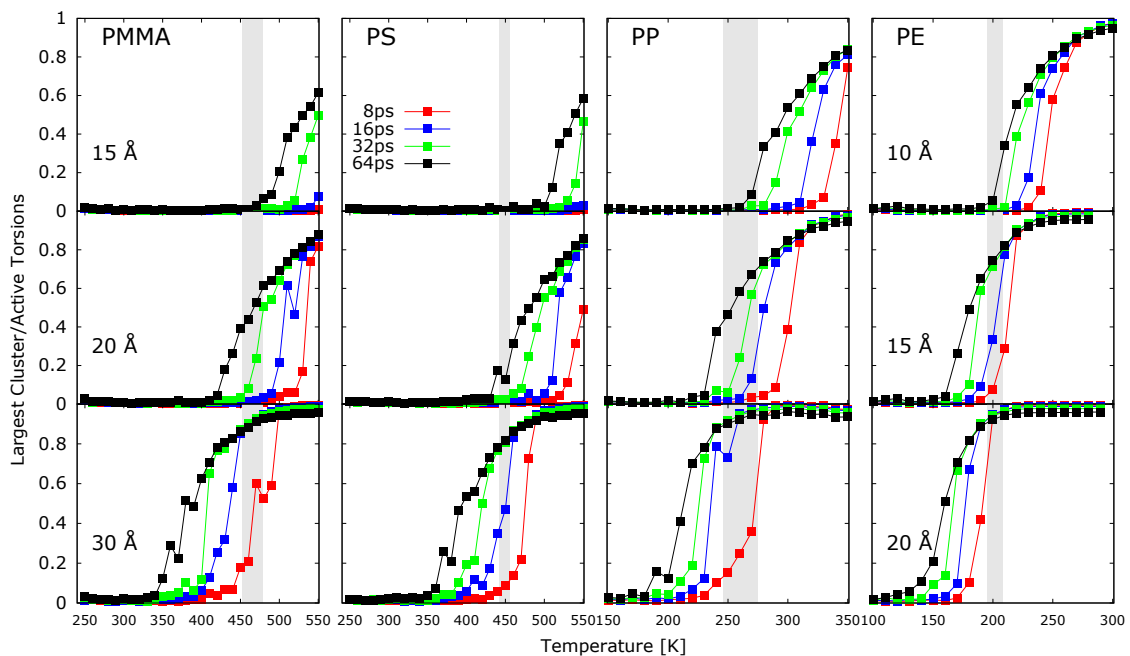


Figure 5.13.: Strength of largest cluster normalized by active torsions as a function of temperature for bulk polymeric samples. clustering analysis performed with various time and spatial cutoffs. The critical temperature for percolation of clusters is around the glass transition temperature across all samples

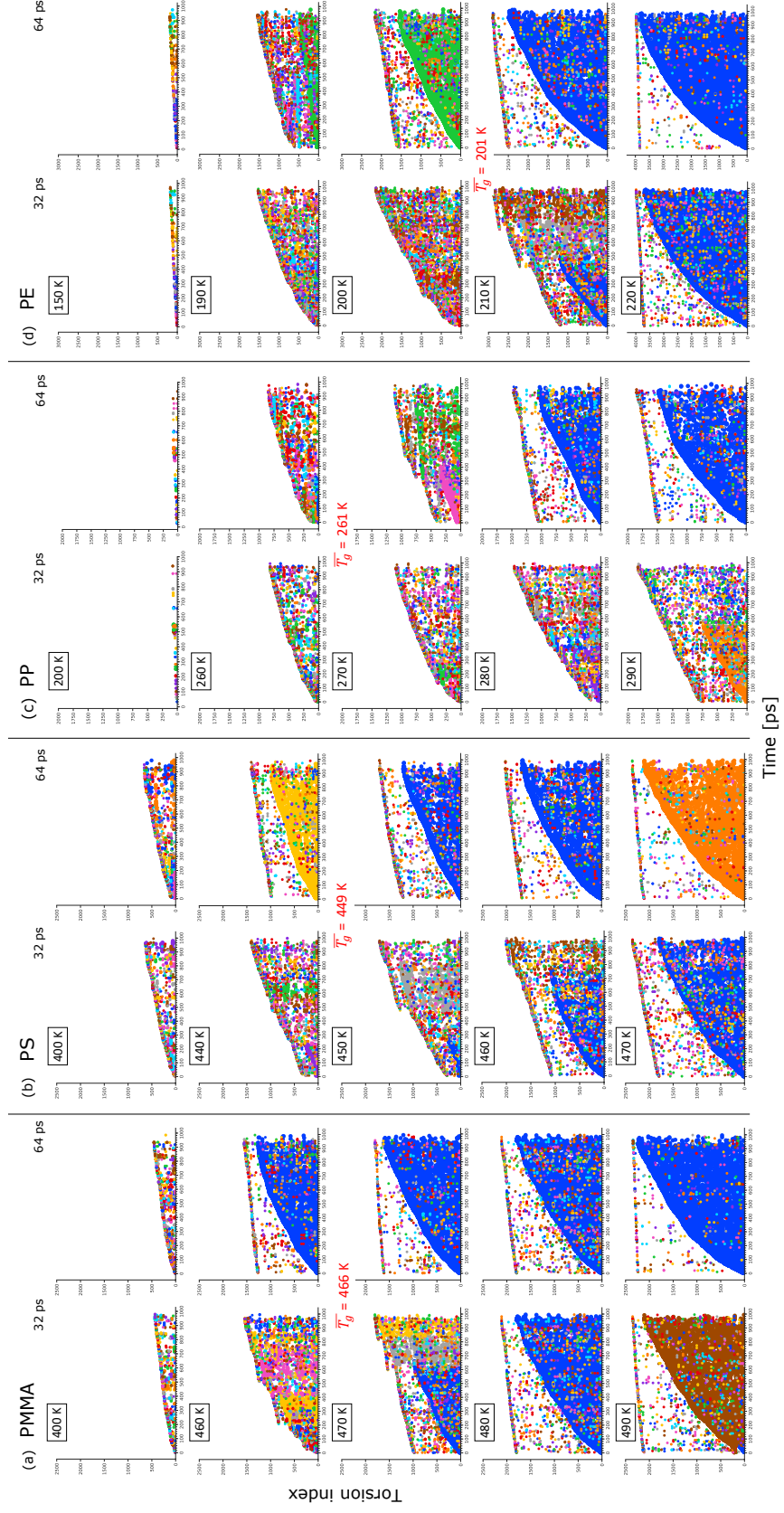


Figure 5.14.: Torsions in order of appearance as a function of time, colored by cluster near T_g in bulk samples; (a) PMMA, (b) PS, (c) PP and, (d) PE

5.4 Role of Chain Molecular Weight and Size Effects in Torsional Relaxation

In this section, we describe the dynamics of PMMA samples with different chain molecular weights and finite size characteristics using the same methodology used in Section 5.3. Our goal is to characterize spatio-temporal high-mobility domains in PMMA systems with free surfaces and to compare their behavior with respect to sizes and to compare their behavior with bulk systems.

The samples studied are: a second bulk system containing 4 chains each 1000 monomers long, a slab of 40 chains with 60 monomers each and two isolated chains: 100 and 1000 monomers long.

The density vs temperature data and corresponding glass transition temperature for both bulk and polymer slab can be found in Fig. 5.15a; alongside conformational rates as a function of temperature are displayed in Fig. 5.15b. They show negligible effects of chain molecular weight in the bulk. The presence of free surfaces in the slab and freestanding chains increases the torsional transition rates.

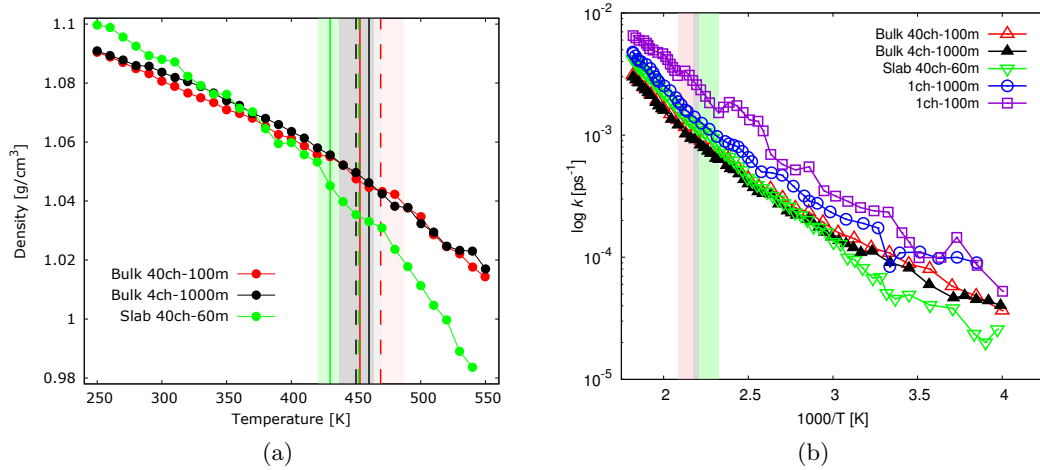


Figure 5.15.: (a) Density vs. Temperature for bulk samples of 40 chains and 4 chains and slab system with 40 chains of PMMA, and (b) Arrhenius plot of conformational transition rates vs temperature for PMMA samples

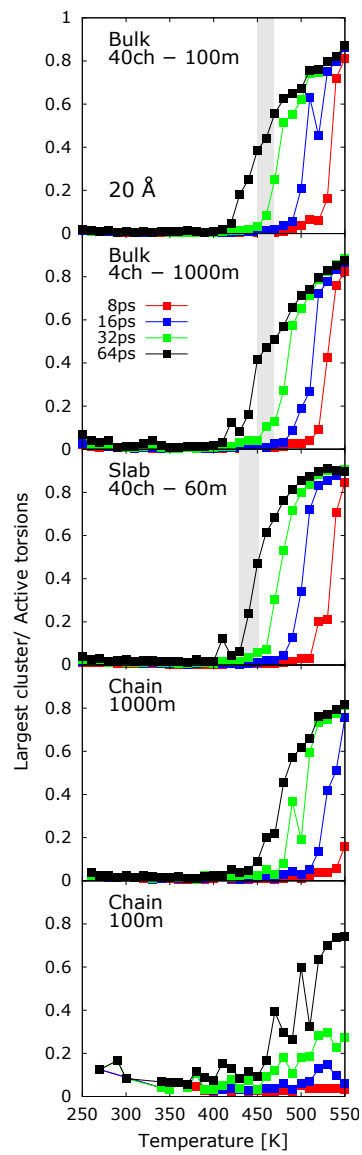


Figure 5.16.: Largest cluster normalized by active torsions as a function of temperature at different time cutoffs with spatial correlation for poly(methyl-methacrylate) samples including finite size geometries

Figure 5.16 shows the strength of the largest cluster for all systems using spatial cutoff of 20 Å. The new bulk system (4 chains, 1000 monomers each) shows no significant difference with the results obtained for the previous reported bulk sample with smaller chain molecular weight which indicates weak dependence of the relaxation dynamics on molecular weight for the range studied. Quite interestingly, the dynamics of the spatio-temporal high-mobility cluster in the polymer slab (with thickness 26 nm) display the same characteristics as the bulk samples. Despite higher overall torsional transition rates, the percolation behavior is nearly identical.

Even more striking is the fact that the isolated chains also exhibit quite similar behavior, indicating that some features of the glass transition and glassy state are retained to very small sized systems. We note that percolation occurs at slightly higher temperatures in isolated chain systems, one could naively interpret this as an increase in T_g , but the reason is simply that these systems are lower density and torsions are further apart from each other. This is particularly true in the smallest, 100-monomer, system.

A picture of the cluster evolution formed at 20 Å and with time cutoff of 32 and 64 ps in the glass transition regime (450 K – 470 K) and at 400 K below T_g is shown in Figure 5.17 for the 4 chain-bulk, slab and isolated chains. The correlated behavior of active torsions at higher temperatures forming one big cluster observed is confirmed in the latter. As the temperature decreases the formation of small clusters remains at later times with the participation of torsion that were previously inactive, by reaffirming the effect that domains of high mobility torsions induce the motion of nearby torsions, in combination with the freezing of the system.

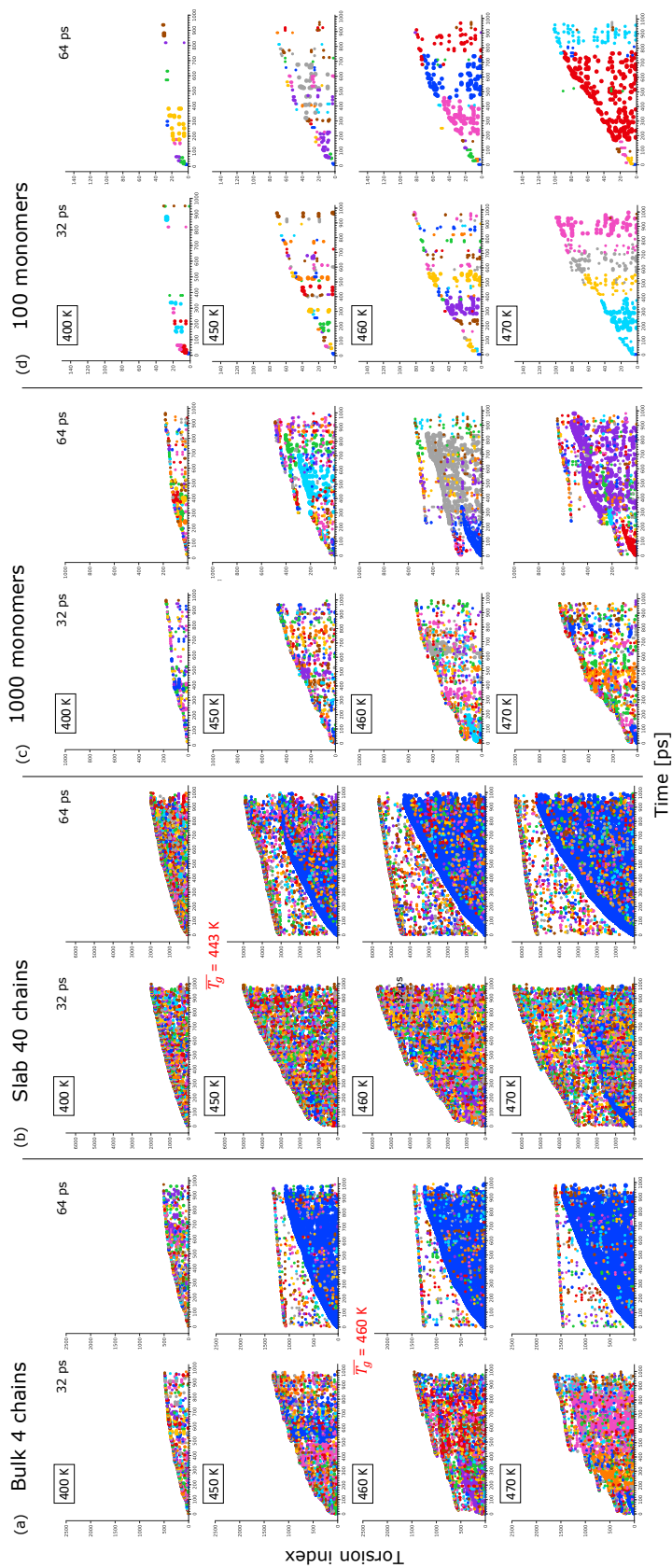


Figure 5.17.: Cluster evolution in the vicinity of T_g for PMMA samples. Torsion index labeled in order of appearance in time

5.5 Universality of Critical Exponents from High-Mobility Domains

Systems undergoing critical phenomena are known to exhibit universal behavior, e.g. while the percolation threshold of various models is system-specific, the critical exponents that describe the system near the phase transition are universal within classes. An important critical exponent, denoted β , measures how the order parameter describing the transformation, strength of the largest cluster in our case, increases as a function of a scaled free parameter (temperature in our case).

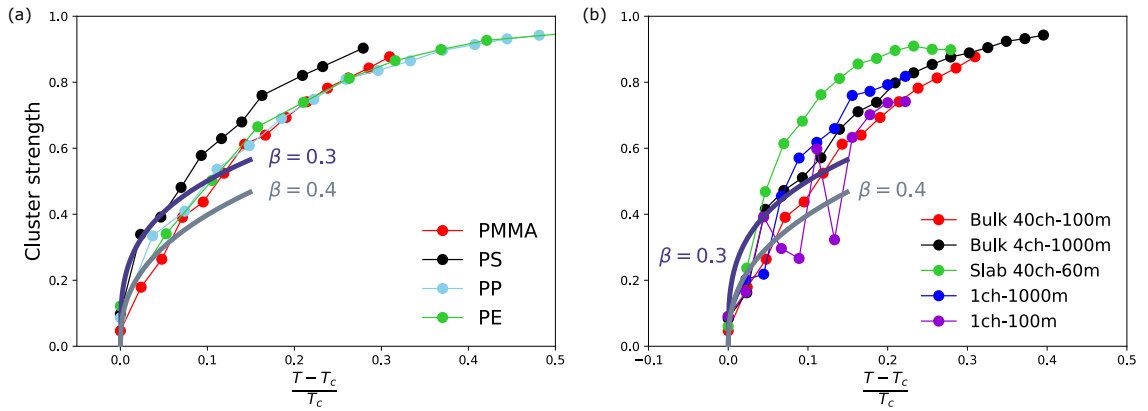


Figure 5.18.: Critical exponents in percolation of high-mobility domains for (a) bulk polymers and (b) PMMA samples

In Figure 5.18 shows the order parameter as a function of normalized temperature above a critical value, T_c , denoting percolation for bulk polymers and PMMA samples. To aid the eye, we also include power law behavior $f(T) \propto (T - T_c)^\beta$ expected in critical processes with exponent $\beta = 0.3$ and 0.4 . While extracting accurate exponent from MD simulations is challenging due to large fluctuations associated with small systems (especially close to T_c where the power law applies) all systems exhibit nearly identical behavior with an exponent β between 0.3 and 0.4 . These values of critical exponent β are similar to those associated with systems undergoing similar phase transformations. Critical exponent β for liquid-gas has been reported to be 0.32 this value also corresponds to the spontaneous magnetization of the three-dimensional Ising model on a cubic lattice. In other problems, such as standard percolation on 3d simple cubic lattice the critical exponent has been

found to be 0.41. We stress that this universal behavior is observed even when the critical temperatures and the rates of torsional transitions are strongly system dependent.

5.6 Conclusions

In summary, we characterized spatio-temporal domains of high mobility in various polymers across their glass transition temperature. We performed a spatio-temporal cluster analysis on backbone torsions that undergo transitions between equilibrium states in several bulk polymers, thin slabs and isolated chains. Prior work had established the relationship between torsional relaxation and the glass transition. Our simulations revealed that the glass transition is marked by the percolation of these high-mobility domains. Quite interestingly, we find identical percolation phenomena, with identical critical exponent, across four different polymers, a thin slab and isolated chain samples, even when transition rates are markedly different in all these systems.

REFERENCES

- [1] US White House Office of Science and Technology Policy. Materials Genome Initiative for Global Competitiveness. Technical report, 2011.
- [2] Juan J. de Pablo, Nicholas E Jackson, Michael A Webb, Long Qing Chen, Joel E Moore, Dane Morgan, Ryan Jacobs, Tresa Pollock, Darrell G Schlom, Eric S Toberer, James Analytis, Ismaila Dabo, Dean M. DeLongchamp, Gregory A Fiete, Gregory M. Grason, Geoffroy Hautier, Yifei Mo, Krishna Rajan, Evan J. Reed, Efrain Rodriguez, Vladan Stevanovic, Jin Suntivich, Katsuyo Thornton, and Ji Cheng Zhao. New frontiers for the materials genome initiative. *npj Computational Materials*, 5(1):41, 12 2019.
- [3] Gurdaman Khaira, Manolis Doxastakis, Alec Bowen, Jiaying Ren, Hyo Seon Suh, Tamar Segal-Peretz, Xuanxuan Chen, Chun Zhou, Adam F. Hannon, Nicola J. Ferrier, Venkatram Vishwanath, Daniel F. Sunday, Roel Gronheid, R. Joseph Kline, Juan J. De Pablo, and Paul F. Nealey. Derivation of multiple covarying material and process parameters using physics-based modeling of X-ray data. *Macromolecules*, 50(19):7783–7793, 2017.
- [4] Rafael Gómez-Bombarelli, Jorge Aguilera-Iparraguirre, Timothy D. Hirzel, David Duvenaud, Dougal Maclaurin, Martin A. Blood-Forsythe, Hyun Sik Chae, Markus Einzinger, Dong Gwang Ha, Tony Wu, Georgios Markopoulos, Soonok Jeon, Hosuk Kang, Hiroshi Miyazaki, Masaki Numata, Sunghun Kim, Wenliang Huang, Seong Ik Hong, Marc Baldo, Ryan P. Adams, and Aln Aspuru-Guzik. Design of efficient molecular organic light-emitting diodes by a high-throughput virtual screening and experimental approach. *Nature Materials*, 15(10):1120–1127, 2016.
- [5] R. Hermann. Performance of materials for aircraft fuselage windows. *Materials and Design*, 9(6):339–342, 1988.
- [6] Takahiro Namazu. Uniaxial tensile test for MEMS materials. In Toshiyuki Tabata, Osamu Tsuchiya, editor, *Reliability of MEMS*, chapter 4, pages 123–161. WileyVCH, 2008.
- [7] Robert A. Riggelman, Gregory N. Toepperwein, George J. Papakonstantopoulos, and Juan J. de Pablo. Dynamics of a glassy polymer nanocomposite during active deformation. *Macromolecules*, 42(10):3632–3640, 5 2009.
- [8] Joshua Mullins, You Ling, Sankaran Mahadevan, Lin Sun, and Alejandro Strachan. Separation of aleatory and epistemic uncertainty in probabilistic model validation. *Reliability Engineering & System Safety*, 147:49–59, 3 2016.
- [9] Ivano E. Castelli, Falco Hüser, Mohnish Pandey, Hong Li, Kristian S. Thygesen, Brian Seger, Anubhav Jain, Kristin A. Persson, Gerbrand Ceder, and Karsten W. Jacob-

- sen. New light-harvesting materials using accurate and efficient bandgap calculations. *Advanced Energy Materials*, 5(2):1400915, 1 2015.
- [10] Nicolas Onofrio, David Guzman, and Alejandro Strachan. Novel doping alternatives for single-layer transition metal dichalcogenide. *Journal of Applied Physics*, 122(18):185102, 11 2017.
 - [11] Alexey V. Lyulin, Nikolaj K. Balabaev, and M. A.J. Michels. Molecular-weight and cooling-rate dependence of simulated Tg for amorphous polystyrene. *Macromolecules*, 36(22):8574–8575, 2003.
 - [12] Paul N. Patrone, Andrew Dienstfrey, Andrea R. Browning, Samuel Tucker, and Stephen Christensen. Uncertainty quantification in molecular dynamics studies of the glass transition temperature. *Polymer*, 87:246–259, 3 2016.
 - [13] John Cologne and Richard Sposto. Smooth piecewise linear regression splines with hyperbolic covariates. *Journal of Applied Statistics*, 21(4):221–233, 1994.
 - [14] R. N. Haward and R. J. Young, editors. *The physics of glassy polymers*. Springer Science+Business Media, 2 edition, 1997.
 - [15] K.J. Rao. The glassy state. In *Structural Chemistry of Glasses*, chapter 2, pages 13–76. Elsevier Ltd, 2002.
 - [16] Gerold Adam and Julian H. Gibbs. On the Temperature Dependence of Cooperative Relaxation Properties in GlassForming Liquids. *The Journal of Chemical Physics*, 43(1):139–146, 7 1965.
 - [17] Marcus T. Cicerone and M. D. Ediger. Relaxation of spatially heterogeneous dynamic domains in supercooled ortho-terphenyl. *The Journal of Chemical Physics*, 103(13):5684–5692, 10 1995.
 - [18] M. D. Ediger. Spatially Heterogeneous Dynamics in supercooled Liquids. *Annual Review of Physical Chemistry*, 51(1):99–128, 10 2000.
 - [19] S. Franz and G. Parisi. Comment on "Dynamical heterogeneities in a supercooled Lennard-Jones liquid". *Physical Review Letters*, 79(15):2827, 4 1998.
 - [20] Christoph Bennemann, Claudio Donati, Jrg Baschnagel, and Sharon C. Glotzer. Growing range of correlated motion in a polymer melt on cooling towards the glass transition. *Nature*, 399:246–249, 1999.
 - [21] Claudio Donati, Sharon C. Glotzer, Peter H. Poole, Walter Kob, and Steven J. Plimpton. Spatial correlations of mobility and immobility in a glass-forming Lennard-Jones liquid. *Physical Review E*, 60(3):3107–3119, 9 1999.
 - [22] Ryoichi Yamamoto and Akira Onuki. Heterogeneous diffusion in highly supercooled liquids. *Physical Review Letters*, 81(22):4915–4918, 11 1998.
 - [23] Hideyuki Mizuno and Ryoichi Yamamoto. Dynamical heterogeneity in a highly supercooled liquid: Consistent calculations of correlation length, intensity, and lifetime. *Physical Review E*, 84(1):1–11, 2011.

- [24] Hung K. Nguyen, Dong Wang, Thomas P. Russell, and Ken Nakajima. Observation of dynamical heterogeneities and their time evolution on the surface of an amorphous polymer. *Soft Matter*, 11(7):1425–1433, 2015.
- [25] Mary J. Burroughs, Dane Christie, Laura A. G. Gray, Mithun Chowdhury, and Rodney D. Priestley. 21st century advances in fluorescence techniques to characterize glass-forming polymers at the nanoscale. *Macromolecular Chemistry and Physics*, 219(3):1700368, 2 2018.
- [26] U. Tracht, M. Wilhelm, A. Heuer, H. Feng, K. Schmidt-Rohr, and H. W. Spiess. Length scale of dynamic heterogeneities at the glass transition determined by multi-dimensional nuclear magnetic resonance. *Physical Review Letters*, 81(13):2727–2730, 9 1998.
- [27] L. Hong, V.N. Novikov, and A.P. Sokolov. Is there a connection between fragility of glass forming systems and dynamic heterogeneity/cooperativity? *Journal of Non-Crystalline Solids*, 357(2):351–356, 1 2011.
- [28] E. Vidal Russell and N. E. Israeloff. Direct observation of molecular cooperativity near the glass transition. *Nature*, 408(6813):695–698, 12 2000.
- [29] Rodney D. Priestley, Linda J. Broadbelt, John M. Torkelson, and Koji Fukao. Glass transition and alpha-relaxation dynamics of thin films of labeled polystyrene. *Physical Review E*, 75(6):061806, 6 2007.
- [30] Martin Tress, Michael Erber, Emmanuel U. Mapesa, Heiko Huth, Jan Müller, Anatoli Serghei, Christoph Schick, Klaus Jochen Eichhorn, Brigitte Voit, and Friedrich Kremer. Glassy dynamics and glass transition in nanometric thin layers of polystyrene. *Macromolecules*, 43(23):9937–9944, 2010.
- [31] Martin Tress, Emmanuel U. Mapesa, Wilhelm Kossack, Wycliffe K. Kipnusu, Manfred Reiche, and Friedrich Kremer. Glassy dynamics in condensed isolated polymer chains. *Science*, 341(6152):1371–1374, 9 2013.
- [32] Rodney D. Priestley, Christopher J. Ellison, Linda J. Broadbelt, and John M. Torkelson. Structural relaxation of polymer glasses at surfaces, interfaces, and in between. *Science*, 309(5733):456–459, 7 2005.
- [33] L. Berthier, G. Biroli, J.-P. Bouchaud, L. Cipelletti, D. El Masri, D. L’Hôte, Laudie F., and M. Pierno. Direct Experimental Evidence of a Growing Length Scale Accompanying the Glass Transition. *Science*, 310(5755):1797–1800, 12 2005.
- [34] C. Dalle-Ferrier, C. Thibierge, C. Alba-Simionesco, L. Berthier, G. Biroli, J.-P. Bouchaud, F. Ladieu, D. L’Hôte, and G. Tarjus. Spatial correlations in the dynamics of glassforming liquids: Experimental determination of their temperature dependence. *Physical Review E*, 76(4):041510, 10 2007.
- [35] E. Hempel, G. Hempel, A. Hensel, C. Schick, and E. Donth. Characteristic length of dynamic glass transition near T_g for a wide assortment of glass-forming substances. *The Journal of Physical Chemistry B*, 104(11):2460–2466, 3 2000.
- [36] S. A. Reinsberg, X. H. Qiu, M. Wilhelm, H. W. Spiess, and M. D. Ediger. Length scale of dynamic heterogeneity in supercooled glycerol near T_g. *The Journal of Chemical Physics*, 114(17):7299–7302, 5 2001.

- [37] Bidur Rijal, Laurent Delbreilh, and Allisson Saiter. Dynamic heterogeneity and cooperative length scale at dynamic glass transition in glass forming liquids. *Macromolecules*, 48(22):8219–8231, 11 2015.
- [38] Zhaohui Yang, Yoshihisa Fujii, Fuk Kay Lee, Chi-hang Hang Lam, and Ophelia K.C. C Tsui. Glass transition dynamics and surface layer mobility in unentangled polystyrene films. *Science*, 328(5986):1676–1679, 6 2010.
- [39] Z. Fakhraai and J. A. Forrest. Measuring the surface dynamics of glassy polymers. *Science*, 319(5863):600–604, 2 2008.
- [40] Simone Napolitano and Michael Wübbenhorst. Structural relaxation and dynamic fragility of freely standing polymer films. *Polymer*, 51(23):5309–5312, 10 2010.
- [41] Keewook Paeng, Stephen F. Swallen, and M. D. Ediger. Direct measurement of molecular motion in freestanding polystyrene thin films. *Journal of the American Chemical Society*, 133(22):8444–8447, 6 2011.
- [42] Y. Gebremichael, T. B. Schröder, F. W. Starr, and S. C. Glotzer. Spatially correlated dynamics in a simulated glass-forming polymer melt: Analysis of clustering phenomena. *Physical Review E*, 64(5):13, 10 2001.
- [43] G. A. Appignanesi, J. A. Rodríguez Fris, R. A. Montani, and W. Kob. Democratic particle motion for metabasin transitions in simple glass formers. *Physical Review Letters*, 96(5):057801, 2 2006.
- [44] Aaron S. Keys, Lester O. Hedges, Juan P. Garrahan, Sharon C. Glotzer, and David Chandler. Excitations Are Localized and Relaxation Is Hierarchical in Glass-Forming Liquids. *Physical Review X*, 1(2):1–15, 2011.
- [45] Arlette R.C. Baljon, Joris Billen, and Rajesh Khare. Percolation of immobile domains in supercooled thin polymeric films. *Physical Review Letters*, 93(25):1–4, 2004.
- [46] Richard H. Boyd, Richard H. Gee, Jie Ran, and Yong Jin. Conformational dynamics in bulk polyethylene: a molecular dynamics simulation study. *The Journal of Chemical Physics*, 101(1):788–797, 1994.
- [47] Yong Jin and Richard H. Boyd. Subglass chain dynamics and relaxation in polyethylene: A molecular dynamics simulation study. *The Journal of Chemical Physics*, 108(23):9912–9923, 6 1998.
- [48] Manel Canales and Gemma Sesé. On the analysis of conformational dynamics in polymers with several rotational isomers. *The Journal of Chemical Physics*, 125(5):054906, 8 2006.
- [49] Xiang Yu, Rongliang Wu, and Xiaozhen Yang. Molecular dynamics study on glass transitions in atactic-polypropylene bulk and freestanding thin films. *The Journal of Physical Chemistry B*, 114(15):4955–4963, 2010.
- [50] Rongliang Wu, Xinlong Qiu, Tianyi Zhang, Kangyu Fu, and Xiaozhen Yang. Atomistic molecular insight into the time dependence of polymer glass transition. *The Journal of Physical Chemistry B*, 119(30):9959–9969, 7 2015.
- [51] François Godey, Alexandre Fleury, and Armand Soldera. Local dynamics within the glass transition domain. *Scientific Reports*, 9(1):1–9, 2019.

- [52] Rongliang Wu, Bin Kong, and Xiaozhen Yang. Conformational transition characterization of glass transition behavior of polymers. *Polymer*, 50(14):3396–3402, 2009.
- [53] Alejandro Strachan. From atoms to materials, 2013.
- [54] Yi Wang and J. Andrew McCammon. Introduction to molecular dynamics: theory and applications in biomolecular modeling. In Nikolay V Dokholyan, editor, *Computational Modeling of Biological Systems*, Biological and Medical Physics, Biomedical Engineering, chapter 1, pages 3–30. Springer US, Boston, MA, 2012.
- [55] Julian H. R. Clarke. Molecular dynamics of glassy polymers. In Kurt Binder, editor, *Monte Carlo and Molecular Dynamics Simulations in Polymer Science*, volume 4, page 608. Oxford University Press, New York, 1995.
- [56] Stephen L. Mayo, Barry D. Olafson, and William A. Goddard. DREIDING: a generic force field for molecular simulations. *The Journal of Physical Chemistry*, 94(26):8897–8909, 12 1990.
- [57] H. Sun. COMPASS: An ab Initio force-field optimized for condensed-phase applications - Overview with details on Aakane and benzene compounds. *The Journal of Physical Chemistry B*, 102(38):7338–7364, 1998.
- [58] Eugenio Jaramillo, Nathaniel Wilson, Stephen Christensen, Jonathan Gosse, and Alejandro Strachan. Energy-based yield criterion for PMMA from large-scale molecular dynamics simulations. *Physical Review B*, 85(2):024114, 1 2012.
- [59] Chunyu Li and Alejandro Strachan. Molecular dynamics predictions of thermal and mechanical properties of thermoset polymer EPON862/DETDA. *Polymer*, 52(13):2920–2928, 2011.
- [60] R. A. Buckingham. The classical equation of state of gaseous helium, neon and argon. *Proceedings of the Royal Society of London. Series A. Mathematical and Physical Sciences*, 168(933):264–283, 1938.
- [61] Carlos Miguel Patiño, Lorena Alzate-Vargas, Chunyu Li, Benjamin P. Haley, and Alejandro Strachan. LAMMPS data-file generator, 2018.
- [62] Noel M O Boyle, Michael Banck, Craig A James, Chris Morley, Tim Vandermeersch, and Geoffrey R Hutchison. Open Babel: An open chemical toolbox. *Journal of Cheminformatics*, 3(33):1–14, 2011.
- [63] Alexander Stukowski. Visualization and analysis of atomistic simulation data with OVITOthe Open Visualization Tool. *Modelling and Simulation in Materials Science and Engineering*, 18(1):015012, 1 2010.
- [64] Benjamin P. Haley, Nate Wilson, Chunyu Li, Andrea Arguelles, Eugenio Jaramillo, and Alejandro Strachan. Polymer modeler, 2015.
- [65] Benjamin P. Haley, Chunyu Li, Nathaniel Wilson, Eugenio Jaramillo, and Alejandro Strachan. Atomistic simulations of amorphous polymers in the cloud with Polymer-Modeler. *arXiv e-prints*, pages 1–30, 3 2015.
- [66] G. B. Olson. Genomic materials design: The ferrous frontier. *Acta Materialia*, 61(3):771–781, 2013.

- [67] Lorena Alzate-Vargas, Chunyu Li, Benjamin P. Haley, Michael E. Fortunato, Coray M. Colina, and Alejandro Strachan. Uncertainties of parameters to predictions of polymer properties by molecular simulations. In *American Society for Composites 2017*, Lancaster, PA, 11 2017. DEStech Publications, Inc.
- [68] Lorena Alzate-Vargas, Michael E. Fortunato, Benjamin Haley, Chunyu Li, Coray M. Colina, and Alejandro Strachan. Uncertainties in the predictions of thermo-physical properties of thermoplastic polymers via molecular dynamics. *Modelling and Simulation in Materials Science and Engineering*, 26(6):065007, 7 2018.
- [69] Johann Gasteiger and Mario Marsili. A new model for calculating atomic charges in molecules. *Tetrahedron Letters*, 19(34):3181–3184, 1978.
- [70] Michael E. Fortunato and Coray M. Colina. pysimm: A python package for simulation of molecular systems. *SoftwareX*, 6:7–12, 2017.
- [71] Steven J. Plimpton. Fast parallel algorithms for short-range molecular dynamics. *Journal of Computational Physics*, 117(1):1–19, 3 1995.
- [72] K Levenberg. A method for the solution of certain non-linear problems in least squares. *Quarterly Journal of Applied Mathematics*, 2(2):164–168, 1944.
- [73] D Montgomery. *Design and analysis of experiments*. John Wiley & Sons, Inc, 5 edition, 2001.
- [74] Harvey Motulsky and Arthur Christopoulos. *Fitting models to biological data using linear and nonlinear regression*. GraphPad Software Inc., San Diego, 1 edition, 2004.
- [75] Hisao Takeuchi and RyongJoon Roe. Molecular dynamics simulation of local chain motion in bulk amorphous polymers. I. Dynamics above the glass transition. *The Journal of Chemical Physics*, 94(11):7446–7457, 1991.
- [76] Bobby G. Sumpter, Donald W. Noid, and Bernhard Wunderlich. Computer experiments on the internal dynamics of crystalline polyethylene: Mechanistic details of conformational disorder. *The Journal of Chemical Physics*, 93(9):6875–6889, 11 1990.
- [77] John D. Ferry. *Viscoelastic properties of polymers*. Wiley, New York, 3 edition, 1980.
- [78] M. D. Ediger, C. A. Angell, and Sidney R. Nagel. Supercooled liquids and glasses. *The Journal of Physical Chemistry*, 100(31):13200–13212, 1 1996.
- [79] Chunyu Li, Alejandro Strachan, Grigori A. Medvedev, Eun-Woong Woong Lee, Jae-woo Kim, James M. Caruthers, and Alejandro Strachan. Molecular dynamics simulations and experimental studies of the thermomechanical response of an epoxy thermoset polymer. *Polymer*, 53(19):4222–4230, 8 2012.
- [80] Robert Simha and R. F. Boyer. On a general relation involving the glass temperature and coefficients of expansion of polymers. *The Journal of Chemical Physics*, 37(5):1003–1007, 9 1962.
- [81] J. Brandrup, Edmund H.; Immergut, Eric A. Grulke, Akihiro Abe, and Daniel R. Bloch, editors. *Polymer handbook*. John Wiley & Sons, New York, 4 edition, 1999.
- [82] Yifu Ding, A. Kisluk, and A. P. Sokolov. When does a molecule become a polymer? *Macromolecules*, 37(1):161–166, 2004.

- [83] A. P. Sokolov, V. N. Novikov, and Y. Ding. Why many polymers are so fragile. *Journal of Physics: Condensed Matter*, 19(20):205116, 5 2007.
- [84] Michael Rubinstein and Ralph H. Colby. *Polymer physics*. OUP Oxford, 1 edition, 2003.
- [85] Rolf Auhl, Ralf Everaers, Gary S. Grest, Kurt Kremer, and Steven J. Plimpton. Equilibration of long chain polymer melts in computer simulations. *The Journal of Chemical Physics*, 119(24):12718–12728, 2003.
- [86] A. J. Hill and M. R. Tant. The structure and properties of glassy polymers. In *In Structure and Properties of Glassy Polymers*, chapter 1, pages 306–325. American Chemical Society, 1999.
- [87] C. A. Angell, K. L. Ngai, G. B. McKenna, P. F. McMillan, and S. W. Martin. Relaxation in glassforming liquids and amorphous solids. *Journal of Applied Physics*, 88(6):3113–3157, 9 2000.
- [88] Taining Liang, Yong Yang, Dawei Guo, and Xiaozhen Yang. Conformational transition behavior around glass transition temperature. *The Journal of Chemical Physics*, 112(4):2016–2020, 1 2000.
- [89] Mitsuhiro Fukuda and Hiroaki Kikuchi. Chain dynamics and conformational transition in cis-polyisoprene: Comparison between melt and subglass state by molecular dynamics simulations. *The Journal of Chemical Physics*, 113(10):4433–4443, 9 2000.
- [90] Zhi Hui Loh, Asim Kumar Samanta, and Paul Wan Sia Heng. Overview of milling techniques for improving the solubility of poorly water-soluble drugs. *Asian Journal of Pharmaceutical Sciences*, 10(4):255–274, 2014.
- [91] J.Y. Huang, H. Yasuda, and H. Mori. Deformation-induced amorphization in ball-milled silicon. *Philosophical Magazine Letters*, 79(6):305–314, 6 1999.
- [92] J. F. Willart and M. Descamps. Solid State Amorphization of Pharmaceuticals. *Molecular Pharmaceutics*, 5(6):905–920, 12 2008.
- [93] He Zhao, Xiaolin Li, Yichi Zhang, Linda S. Schadler, Wei Chen, and L. Catherine Brinson. Perspective: NanoMine: A material genome approach for polymer nanocomposites analysis and design. *APL Materials*, 4(5), 2016.
- [94] Yifei Zeng, Lorena Alzate-Vargas, Chunyu Li, Rachel Graves, Jeff Brum, Alejandro Strachan, and Marisol Koslowski. Mechanically induced amorphization of small molecule organic crystals. *Modelling and Simulation in Materials Science and Engineering*, 27(7):074005, 10 2019.
- [95] Anthony K. Rappé, William A. Goddard III, Anthony K. Rappe, and William A. Goddard III. Charge equilibration for molecular dynamics. *The Journal of Physical Chemistry*, 95(8):3358–3363, 1991.
- [96] Chunyu Li and Alejandro Strachan. Molecular simulations of crosslinking process of thermosetting polymers. *Polymer*, 51(25):6058–6070, 2010.
- [97] Minoru Yoshioka, Bruno C. Hancock, and George Zografi. Crystallization of indomethacin from the amorphous state below and above its glass transition temperature. *Journal of Pharmaceutical Sciences*, 83(12):1700–1705, 12 1994.

- [98] T. Beyer, G. M. Day, and S. L. Price. The prediction, morphology, and mechanical properties of the polymorphs of paracetamol. *Journal of the American Chemical Society*, 123(21):5086–5094, 2001.
- [99] Thomas J. Kistenmacher and Richard E. Marsh. Crystal and molecular structure of an antiinflammatory agent, indomethacin, 1-(p-Chlorobenzoyl)-5-methoxy-2-methylindole-3-acetic acid. *Journal of the American Chemical Society*, 94(4):1340–1345, 1972.
- [100] P. J. Wheatley. The crystal and molecular structure of Aspirin. *Journal of the Chemical Society*, 6036:6036–6048, 1964.
- [101] Russell D.L. Johnstone, Alistair R. Lennie, Stewart F. Parker, Simon Parsons, Elna Pidcock, Patricia R. Richardson, John E. Warren, and Peter A. Wood. High-pressure polymorphism in salicylamide. *CrystEngComm*, 12(4):1065–1078, 2010.
- [102] C. A. Beevers, T. R. R. McDonald, J. H. Robertson, and F. Stern. The crystal structure of sucrose. *Acta Crystallographica*, 5(5):689–690, 1952.
- [103] Qi-Jun Jun Hong and Axel van de Walle. Solid-liquid coexistence in small systems: A statistical method to calculate melting temperatures. *The Journal of Chemical Physics*, 139(9):094114, 9 2013.
- [104] R. Candelier, O. Dauchot, and G. Biroli. Building blocks of dynamical heterogeneities in dense granular media. *Physical Review Letters*, 102(8):1–4, 2 2009.
- [105] R. Candelier, A. Widmer-Cooper, J. K. Kummerfeld, O. Dauchot, G. Biroli, P. Harrowell, and D. R. Reichman. Spatiotemporal hierarchy of relaxation events, dynamical heterogeneities, and structural reorganization in a supercooled liquid. *Physical Review Letters*, 105(13):135702, 9 2010.
- [106] Aaron S. Keys, Adam R. Abate, Sharon C. Glotzer, and Douglas J. Durian. Measurement of growing dynamical length scales and prediction of the jamming transition in a granular material. *Nature Physics*, 3(4):260–264, 4 2007.
- [107] Rishikesh K. Bharadwaj and Richard H. Boyd. Effect of pressure on conformational dynamics in polyethylene: A molecular dynamics simulation study. *Macromolecules*, 33(16):5897–5905, 8 2000.
- [108] A. Soldera and N. Metatla. Study of the glass transition temperatures of stereoregular PMMAs using different force fields. *Internet Electronic Journal of Molecular Design*, 4:721–736, 2005.
- [109] Dietrich Stauffer and Amnon Aharony. *Introduction to percolation theory*. Taylor & Francis, Philadelphia, 2 edition, 1994.

VITA

Lorena Alzate-Vargas obtained her Ph.D. from the Material Engineering Department at Purdue University in 2019 under the supervision of Prof. Alejandro Strachan. Previously, Lorena obtained her B.S in 2014 in Engineering Physics from Universidad EAFIT - Medellin, Colombia under the supervision of Profs. Jorge David and Mario Velez. During her Ph.D. at Purdue, Lorena focused on the understanding of conformational dynamics and the nature of the glass transition in polymeric materials, from molecular simulations. In addition to her work as a researcher, during her Ph.D., Lorena has helped in the development of scientific tools, python notebooks, and other tutorials in the nanoHUB platform to facilitate the use of classical molecular dynamics simulations in polymers to a wide range of users from undergraduate students to scientists.